A 667-year record of co-seismic and interseismic Coulomb stress changes in central Italy reveals the role of fault interaction in controlling irregular earthquake recurrence intervals

L. N. J. Wedmore[1,5], J. P. Faure Walker[1], G. P. Roberts[2], P. R. Sammonds[1], K. J. W McCaffrey[3], P. A. Cowie[4]

[1]Institute for Risk and Disaster Reduction, University College London, Gower Street, London, WC1E 6BT, UK

[2]Department of Earth and Planetary Sciences, Birkbeck, University of London, WC1E 6BX, UK

[3]Department of Earth Sciences, Durham University, South Road, Durham, DH1 3LE, UK

[4]Department of Earth Science, University of Bergen, Bergen 5002, Norway

[5]Now at Institute of Geophysics and Tectonics, University of Leeds, Leeds, LS2 9JT, UK

Corresponding author: Luke Wedmore (l.wedmore@leeds.ac.uk)

Key Points:

- **We model elastic stress interactions for 30 earthquakes on 97 faults over 667 years in central Italy**
- **Co-seismic Coulomb stresses can cause earthquake inter-event times changes for individual faults on the order of 10^3 years**
- **Coulomb stress changes cause shorter faults to experience more irregular earthquake recurrence intervals and greater slip rate variability**

This article has been accepted for publication and undergone full peer review but has not been through the copyediting, typesetting, pagination and proofreading process which may lead to differences between this version and the Version of Record. Please cite this article as doi: 10.1002/2017JB014054

Abstract

Current studies of fault interaction lack sufficiently long earthquake records and measurements of fault slip-rates over multiple seismic cycles to fully investigate the effects of interseismic loading and co-seismic stress changes on the surrounding fault network. We model elastic interactions between 97 faults from 30 earthquakes since 1349 AD in central Italy to investigate the relative importance of co-seismic stress changes versus interseismic stress accumulation for earthquake occurrence and fault interaction. This region has an exceptionally long, 667-year record of historical earthquakes and detailed constraints on the locations and slip-rates of its active normal faults. Of 21 earthquakes since 1654, 20 events occurred on faults where combined co-seismic and interseismic loading stresses were positive even though ~20% of all faults are in 'stress shadows' at any one time. Furthermore, the Coulomb stress on the faults that experience earthquakes is statistically different from a random sequence of earthquakes in the region. We show how co-seismic Coulomb stress changes can alter earthquake inter-event times by c.10^3 years, and fault length controls the intensity of this effect. Static Coulomb stress changes cause greater inter-event perturbations on shorter faults in areas characterized by lower strain (or slip) rates. The exceptional duration and number of earthquakes we model enable us to demonstrate the importance of combining long earthquake records with detailed knowledge of fault geometries, slip-rates and kinematics to understand the impact of stress changes in complex networks of active faults.

1 Introduction

Advances in high-resolution topography and Quaternary dating tools suggest that transient fault slip rates and irregular earthquake recurrence intervals over thousand year timescales are a common feature of extensional areas [e.g. *Friedrich et al.,* 2004; *Palumbo et al.,* 2004; *Bull et al*., 2006; *Nicol et al*., 2010; *Begg and Mouslopoulou,* 2010; *Akçar et al*., 2012; *Jewell and Bruhn,* 2013; *Nicol et al*., 2016; *Cowie et al*., 2017] as well as other tectonic environments [e.g. *Weldon et al.,* 2004; *Oskin et al.,* 2008; *Dolan et al.,* 2016; *Gold et al.,* 2017]. A number of different processes have been invoked to explain this transient behavior including static elastic stress transfer [*Benedetti et al*., 2013], dynamic (i.e. co-seismic) stress changes [*Brodsky and van der Elst*, 2014], temporal variations in the strength of brittle faults and ductile shear zones [*Dolan et al.,* 2007], fluid migration through fault zones [*Oskin et al*., 2008], interactions with surface processes [*Hetzel and Hampel,* 2005], episodic release of strain stored in a crustal stress "battery" [*Gold et al.,* 2017], and energy dissipation and minimization of work in response to flexural bending of normal fault footwalls [Cowie *et al*.,

2017]. However, the timescales upon which these processes can affect fault slip rates is poorly constrained, and it is not clear which of these processes, if any, are the dominant mechanism controlling transient fault slip rates and irregular earthquake recurrence times. In this paper, we examine the role of elastic Coulomb stress interactions in the variability of fault slip rates and earthquake recurrence times over timescales of 10^3 years.

Elastic interactions between active faults have been invoked to explain a range of observations of fault and earthquake behavior within distributed fault networks including temporal and spatial changes in slip-rates over periods of 10^2-10^5 years [*Cowie et al.*, 2005; *Nicol et al.*, 2010] and triggering of subsequent earthquakes [*King et al.*, 1994]. Numerical modelling of this process is often used to explore the effects of stress interactions on earthquake clustering, variation in recurrence intervals and time varying fault slip-rates [*Robinson*, 2004; *Marzocchi et al.*, 2009; *Robinson et al.*, 2009; *Cowie et al.*, 2012]. However, many of these models are purely theoretical [e.g. *Cowie et al.*, 1993; *Zöller and Hainzl*, 2007] or include only a relatively short record of recent earthquakes [e.g. *Stein et al.*, 1992; *King et al.*, 1994]. Other models lack many of the structural characteristics of fault networks that are thought to be key factors in determining how faults interact such as detailed fault geometry and kinematics, variable slip-rates and interseismic loading rates for different faults, and earthquake histories that contain multiple seismic cycles [e.g. *Robinson*, 2004; *Marzocchi et al.*, 2009; *Robinson et al.*, 2009; *Marzocchi and Melini*, 2014]. Consequently, the characteristics of how faults interact over periods of time longer than individual earthquakes and what affect these longer-term interactions have on current earthquake activity, fault behavior and seismic hazard is poorly understood.

Over timescales of 10^4-10^5 years fault interactions lead to an increase in length and displacement rates on faults that are optimally located and orientated within a diffuse network of extensional faults [*Cowie*, 1998]. Over shorter timescales (10^2-10^3 years) the effects of fault interactions on fault slip-rates and earthquake recurrence intervals are less well understood, but it appears that earthquake activity is clustered both in time and space. Earthquake clusters seen in high-resolution dated stratigraphic sequences in actively extending regions suggest that fault slip-rates vary over timescales of 10^2-10^3 years [e.g. *Bull et al.*, 2006; *Nicol et al.*, 2010]. Evidence from ^{36}Cl cosmogenic exposure dating of bedrock fault scarps produced by normal faulting earthquakes show accelerated fault slip-rates over periods of a few thousand years that are presumably associated with temporal clusters of

earthquakes, alongside periods of quiescence (e.g. *Mitchell et al.* [2001] – Israel; *Palumbo et al.* [2004], *Schlagenhauf et al*. [2011], *Benedetti et al*. [2013],*Tesson et al*. [2016] and *Cowie et al.* [2017] – central Italy; *Benedetti et al.* [2002] – Greece; *Akçar et al.* [2012] – Turkey). Whilst the role of Coulomb stress changes in triggering short term clusters of seismicity is now widely acknowledged [*King et al*., 1994; *Stein et al*., 1997], the role of Coulomb stress changes in causing the sort of regional changes in seismicity over 10^2-10^3 years observed in ^{36}Cl cosmogenic exposure data and high-resolution stratigraphy is less clear.

We use the central Apennines, Italy to explore how faults are interacting through elastic Coulomb stress perturbations. Spatially transient temporal clusters of seismicity in the region over 10^2-10^3 years (Figure 1; *Schlagenhauf et al*. [2011]; *Benedetti et al*. [2013]; *Tesson et al*. [2016]), and shorter term clusters of earthquakes (e.g. The 2016 central Italy earthquake sequence) suggests faults are interacting over a range of timescales. Furthermore, the region has exceptional constraints on (i) the long record of historical earthquakes (Figure 1) which appears to be complete for events M>5.8 since 1349 AD [*Guidoboni et al.*, 2007]; (ii) the constraints on the mechanism controlling fault slip-rates over multiple seismic cycles where slip-rates which appear to be controlled by viscous deformation at depth in response to long wavelength topographic uplift [*Faure Walker et al.*, 2012; *Cowie et al.*, 2013]; (iii) the extensive record of Holocene fault slip-rates in the region where nearly every fault has a slip-rate derived from offset geomorphic features dating from 15 ± 3 ka (Figure 2a) [e.g. *Roberts and Michetti*, 2004; *Faure Walker et al.*, 2010]; and (iv) the extensive record of fault geometries and kinematics across faults in the region (Figure 2b) [*Roberts and Michetti*, 2004; *Faure Walker et al.*, 2009, 2010]. We use these constraints and records of earthquake activity in the central Apennines to model interseismic and co-seismic stress interactions to explore the characteristics of an actively-interacting distributed fault network and to determine whether Coulomb stress changes can explain observations of transient fault slip rates and irregular earthquake recurrence intervals.

2 Tectonics of the central Apennines

Extensional faulting in the central Apennines initiated c. 2-3 Ma as thrusting caused by subduction of the Adriatic plate beneath Italy slowed, and a slab window opened allowing mantle upwelling to become the dominant geodynamic process [*D'Agostino et al.*, 2001; *Faure Walker et al.*, 2012]. This has produced sets of sub-parallel extensional faults up to 40 km in length, distributed over the crest of a long-wavelength topographic high along the axis

of the central Apennine mountain chain that has been uplifted from sea-level to >1000 m elevation since the Pliocene [*D'Agostino et al.*, 2001; *Galadini et al.*, 2003a]. Geodetic extension rates across the central Apennines of 2.9 ± 1 mm yr^{-1} [*D'Agostino et al.*, 2011] broadly match the ~3 mm yr^{-1} maximum extension rate calculated across the region by summation of 15 ± 3 ka strain-rates [*Faure Walker et al.*, 2010]. Upper crustal brittle strain-rates also correlate with areas of high topography, high free air gravity values and maxima in SKS splitting delay times indicating that surface strain rates in the central Apennines across the 80-90km width of the mountain chain are controlled by viscous flow at the base of the seismogenic portion of the crust [*Faure Walker et al.*, 2012; *Cowie et al.*, 2013].

2.1 Faults in the central Apennines

Individual normal faults in the central Apennines offset pre-rift Tertiary and Mesozoic carbonates by up to 2.5 km [*Roberts and Michetti*, 2004]. Following initiation of extension in the Plio-Pleistocene, fault interaction and crustal-scale strain localization led to fault growth and caused an increase in throw rates on the centrally located faults from c. 0.7 Ma [*Roberts et al.*, 2002; *Roberts and Michetti*, 2004; *Whittaker et al.*, 2007]. Offsets of sediments and hillslopes that have been preserved since the last glacial maximum (LGM) have been measured at 174 locations on 48 faults and yield fault throw-rates in the central Apennines averaged over 15 ± 3 ka (Figure 2a; *Roberts and Michetti* [2004]; *Faure Walker et al*, [2010]; *Tucker et al.* [2011]). Measurements of striated and corrugated fault planes at 278 locations (>14,000 individual measurements) constrain the kinematics of the individual faults (Figure 2b) [*Morewood and Roberts*, 2000; *Roberts and Michetti*, 2004; *Faure Walker et al.*, 2010].

2.2 Historical Earthquakes

Since 9th September 1349 AD, the day of 3 well-document large magnitude earthquakes, the historical catalogue of earthquakes in central Italy, which comprises of macroseismic shaking intensities for damaged towns and villages, is thought to be complete for all earthquakes with Me ≥ 5.8 [*Michetti et al*., 1996; *Roberts et al*., 2004; *Guidoboni et al*., 2012]. From 1349 AD, the historical records include 27 large magnitude earthquakes; the shaking of individual towns and villages in each of these earthquakes (where $I_{mcs} \geq$ VIII) is shown in Figure 1b. In addition we include the 2016 earthquake sequence that occurred in the north east of the central Apennines – on the Laga and Mt Vettore faults (Figure 2). We used the historical shaking records (Figure 1b) alongside the palaeoseismic records of faulting in the region (see Table 1 and Table S1), contemporary reports of surface ruptures [e.g. *Blumetti*, 1995; *Cello et*

al., 1997], seismology [e.g. *Westaway et al.*, 1989] and geodetic records [e.g. *Walters et al.*, 2009] to constrain the faults that ruptured in 30 major earthquakes since 1349 AD (Table 1).

Projecting the macroseismic shaking from historical earthquakes since 1349 AD onto a transect perpendicular to the strike of faults in the central Apennines shows that the majority of the activity during this time has occurred on faults on the northeastern side of the region (Figure 1b). In contrast to the asymmetric pattern of post 1349 AD seismicity, Holocene-active faults scarps (Figure 1) and post-LGM strain-rates [*Faure Walker et al.*, 2010, 2012] are more evenly distributed across both sides of the central Apennines, across the crest of the regional long wavelength topographic bulge. To investigate the role of elastic fault interaction in causing this skewed regional seismicity since 1349, we model the historical earthquakes and interseismic loading of faults from 1349-2016 AD to investigate how faults are interacting in the central Apennines, and investigate the effects of these interactions on perturbing earthquake inter-event times.

3 Model Setup

We are interested in determining the elastic stress perturbations caused by earthquakes on surrounding faults in a complex normal fault network due to both co-seismic static stress changes and interseismic loading. For co-seismic stress changes we calculate the change in Coulomb stress (ΔCFF) following each historical earthquake in the central Apennine fault network. The change in Coulomb stress is defined as:

$$\Delta CFF = \Delta\tau + \mu' \Delta\sigma_n \quad (1)$$

where $\Delta\tau$ is the change in shear stress on a fault, $\Delta\sigma_n$ is the change in normal stress on a fault and μ' is the effective coefficient of friction. Shear stress is resolved in the slip direction of each fault and normal stresses are positive if that fault becomes unclamped. We use a value for μ' of 0.4 although our results are not sensitive to the value used within the standard range of 0.2-0.6. The ΔCFF calculations were performed using the *Coulomb 3.3* code [*Lin and Stein*, 2004; *Toda et al.*, 2005] that uses the elastic half-space code of *Okada* [1992].

We model 97 faults in the central Apennines that show evidence of activity since the demise of the LGM as receiver faults. The fault map is constructed from geological maps of the region with evidence for Holocene activity from field mapping of post-LGM geomorphic offsets [*Morewood and Roberts*, 2000; *Cowie and Roberts*, 2001; *Roberts et al.*, 2002;

Roberts and Michetti, 2004; *Papanikolaou et al.*, 2005; *Faure Walker et al.*, 2010, 2012; *Wilkinson et al.*, 2015]. This probably includes all major faults (i.e. with slip rate > ~0.1 mm yr^{-1}) in the region as (a) slip-rates as low as 0.1 mm yr^{-1} would produce cumulative offsets of 100 m over 1 Ma, that would be resolvable on geological maps; (b) if significant contributors to the overall strain were missing then correlations between geodetic and geologic measurements of strain and between strain-rate and topography would not hold [e.g. *D'Agostino et al.*, 2011; *Cowie et al.*, 2013]; and (c) no significant clusters of microseismicity have occurred outside areas surrounding mapped faults during the last 30 years [*Boncio et al.*, 2009].

3.1 Modelling faults, fault geometries and fault kinematics

Faults are modelled as linear features within the elastic half-space model and partitioned into 3 km long sections along strike with 5 sections down dip to a vertical depth of 15 km, constrained by the maximum depth of seismicity measured in the region [*Boncio et al.*, 2009; *Chiarabba et al.*, 2009]. 3km long sections were chosen as this is the approximate resolution along strike at which kinematic and throw-rate measurements have been collected along the faults (Figure 2a). We include the fault kinematics as they can alter the local stress field towards the tips of faults [*Maniatis and Hampel*, 2008]. As fault strike is a controlling factor on fault kinematics, we also correct for the differences between the strike of the mapped faults and the planar fault trace by preserving the principal direction of strain and the magnitude of strain rate (see Text S1, *Faure Walker et al*. [2009] and *Wilkinson et al*. [2015] for details).

3.2 Interseismic stress accumulation

In the central Apennines, *Cowie et al*. [2013] showed that below the seismogenic zone, non-linear viscous deformation dominates and promotes strain localization. Consequently, we load the faults interseismically by continuous creep on shear zones at the base of each fault, below the locked brittle (seismogenic) upper crust (Figure 3). The agreement between modern GPS extension rates and summed 15 ± 3 ka strain rates measured across all faults in the central Apennines indicates there is no overall stress accumulation on the faults at geological timescales [*Faure Walker et al*., 2010]. Therefore, we impose the slip-rates measured at the surface from the offset of 15 ± 3 ka landforms (Figure 2a) onto our modelled shear zones (Figure 3b). We then resolve the stress changes caused by the creeping shear zones onto patches in the upper seismogenic sections of the faults within the elastic half-

space model described above (Figure 3b-c). The advantages of using this method to load the faults are as follows: i) fault specific slip rates can be used as a constraint on the long-term loading rate in such a way that would not be possible if bulk measures of regional strain (e.g. GPS measurements) were used; ii) the approach relates well to physical models that show that in the presence of a brittle-ductile transition down-dip, the viscous layer deforms continuously whereas the brittle layer remains locked between earthquakes [e.g. *Huc et al.* 1998]; and iii) the setup creates an increase in stressing rate with depth such that the whole fault would reach its failure stress at about the same time. An alternative approach to load the brittle fault uniformly down dip would result in disproportionately high levels of stress (and therefore unstable slip) near to the surface not seen in observations of the depth of large earthquakes [e.g. *Das and Scholz*, 1983]. A depth of 15-24 km is used for the creeping shear zones as above this depth deformation occurs through brittle deformation as evidenced by active seismicity and the lower extent falls within the depth range found by *Cowie et al.* [2013] for localized viscous flow.

Throw measurements over 15±3 ka were converted to slip-rates per year for each section along strike using the dip of the modelled faults as calculated above (see Text S1for details of this calculation and Table S2 for fault specific parameters). Slip-rate within the shear zone was assumed to be constant down-dip and zero at the fault tips. The fault kinematics were assumed to match the kinematics of the portion of the fault in the upper crust. The resultant stress transferred reflects the annual interseismic loading stress acting on the fault. An internal check to ensure that the stress loading rates are consistent with earthquake recurrence intervals observed in palaeoseismic trenches is shown in the Section S2 in the supplementary material.

3.3 Modelling co-seismic stress changes from historical earthquakes

Although the time and location of the historical earthquakes is relatively well-known, the slip distributions are poorly constrained by measurements with debate even surrounding the well-studied L'Aquila earthquake in 2009 (see *Wilkinson et al.* [2015] for a summary). Although some earthquake slip-distributions are asymmetrical [*Manighetti et al*., 2005], we use triangular shaped slip distributions to model the historical earthquakes, as normalized finite displacement profiles in the central Apennines, which average the earthquake surface slip distributions over the last 3Ma, show a more symmetrical, triangular shaped displacement profile (Figure 2c). We calculate average slip across the triangular shaped slip distribution

from empirical relationships between magnitude and average slip [*Wells and Coppersmith*, 1994] with the maximum slip centered in the middle of the faults (following *Nalbant et al.* [2013]). Rupture length was calculated using empirical relationships between magnitude and sub-surface rupture length [*Wells and Coppersmith*, 1994]. Where palaeoseismic evidence and contemporary reports suggest multiple fault ruptures (e.g. 14th January 1703 [*Blumetti*, 1995]; 2nd February 1703 [*Galli et al.*, 2010]; 13th January 1915 [*Michetti et al.*, 1996]; 24th August 2016 [*Livio et al.*, 2016]), the empirically calculated rupture lengths were divided among the faults responsible for the earthquake (Figure 2b).

The stress changes on faults at any point in time is the sum of the interseismic and co-seismic stress changes up to that point, starting from immediately prior to the first of the earthquakes in 1349 AD. Stress changes were resolved on all faults in the region (all faults act as receiver faults). Coulomb stress on the portions of the faults that ruptured in each event were re-set to zero.

3.4 Errors and Uncertainties

We apply errors to the magnitudes of earthquakes prior to 1979 as these magnitudes are derived from inversions of macroseismic shaking records [*Gasperini and Ferrari*, 2000]. For earthquakes prior to 1703 AD we use a magnitude uncertainty of ± 0.3. From 1703 AD onwards, when the density of historical records improves, we applied an uncertainty of ± 0.2. These estimates were used to alter the average slip of each event alongside the upper and lower bounds of the *Wells and Coppersmith* [1994] magnitude – average slip scaling law. The maximum magnitude modelled is M=7.0 (considered to be the maximum possible magnitude in the region: see *D'Agostino* [2014]). For two earthquakes (5th December 1456, M=5.8 and 24th July 1654, M=6.4), scenarios were run varying the source fault of each event, as two possible causative faults were indistinguishable given the palaeoseismology and historical macroseismic records available. We included the uncertainty of the time constraint on the fault slip-rate measurements by running interseismic loading models with slip-rates averaged over 12ka, 15ka and 18ka respectively. This results in 36 end-member modelling scenarios by varying: i) the slip-rates used for interseismic loading (3 different scenarios); ii) the faults that ruptured in 1456 and 1654 (4 different scenarios); and iii) the magnitude and average slip of earthquakes (3 different scenarios). These alternative results are shown in Figure S5 and summarized below.

There is uncertainty over whether mean or maximum stress is the best indicator of future large earthquakes (see the debate between the cascade and deterministic models of rupture propagation; *Olson and Allen*, [2005, 2006]; *Rydelek and Horiuchi*, [2006]). We base our decision to analyse the mean Coulomb stress changes on need to account for the stress across the whole fault including the inherent heterogeneous stress distribution created by previous ruptures, closely spaced faults and complex structural barriers [*Aki*, 1984; *Steacy et al.*, 2004; *Bull et al.*, 2006; *Noda et al.*, 2013].The implications of using the mean stress in our analysis is that it will: (i) produce a more generalized view of the long-term behavior of the fault system; (ii) give an impression of the relative likelihood of future *major* earthquakes rather than small events; (iii) mean our results are not overly biased by the slip distribution of the events modelled; and (iv) allow our results to be affected by the realistic structural and kinematic variability we have incorporated in our model.

4 Results

The maximum interseismic Coulomb stress loading rate on any individual fault patch in the upper crust is shown in Figure 3d. Due to the model setup, these loading rates are broadly consistent with the loading rates that may be inferred from palaeoseismic recurrence times (see supplementary material).

Figure 4 and 5 shows the mean Coulomb stress on each fault immediately prior to earthquakes from 1654-2016 AD. This includes the effects of the previous stress changes induced by historical earthquakes from 1349 AD onwards and interseismic loading stresses from 1349 AD onwards. Results are shown from 1654 AD onwards to allow the model to accumulate co-seismic and interseismic stresses such that analysis on the distribution of stresses is performed without starting from a baseline of zero stress on each fault. Figure 6 shows the combined co-seismic and interseismic Coulomb stress on all faults in the central Apennines immediately following the M_w6.6 earthquake on 30th October 2016. The maps in Figure 4 and 5 are summarized in Figure 7a where the mean Coulomb stress on each fault prior to each earthquake is shown. The mean accumulated Coulomb stresses on the faults that subsequently rupture (red circles) are positive and between 0-1 MPa for all but one earthquake: the M=6.0 earthquake in 1933 on the Maiella Fault. However, 5 of the 15 patches of the Maiella Fault that ruptured were experiencing positive stress. Thus, a pattern emerges where earthquakes occur preferentially on faults that remain positively stressed after hundreds of years of interseismic loading and co-seismic loading and unloading, even though

c.20% of faults are in 'stress shadows' at any one time. To test whether this pattern is significant, we calculated the percentile of the stress on the fault that failed in each event relative to the distribution of stresses on each fault. This analysis was performed for each earthquake from 1654 AD onwards and the mean percentile of the fault that failed was calculated. Faults were then randomly selected from the distribution of stresses on all faults for each earthquake from 1654 AD onwards, and the average percentile for this random sequence was then calculated. This random selection was made 10,000 times and the resultant distribution was compared with the mean percentile of failure stress of the actual sequence of events. A non-parametric Mann-Whitney U test was performed to test whether the actual sequence of events was statistically different from the 10,000 random draws. For the modelling scenario shown in Figures 4, 5 and 7a, the value of U was 0.039, indicating that the actual sequence of earthquakes is significantly different from a random sequence of earthquakes at a 95% confidence level. In essence, earthquakes are more likely to occur on faults above the mean Coulomb stress acting on all faults. Crucially, this result holds not just for one earthquake but for 21 earthquakes since 1654.

Figure 7b shows the change in the number of faults through time where the combined accumulated co-seismic and interseismic Coulomb stresses are positive or negative. When summed over time, interseismic stresses (c. 10^{-2}-10^{-3} MPa yr^{-1}) might be expected to dominate the final stress map (Figure 6) and to overcome any (negative) co-seismic stress changes (c. -10^{-1} MPa) after 10-100 years. However, after running our model for 667 years, the co-seismic stress changes have not been overcome, with approximately 20% of faults (20-25 out of 97 faults) being net negatively stressed at any time since 1654 AD. As these negative stresses are only generated within co-seismic 'stress shadows', we investigate the effects that the co-seismic stress changes for all 30 earthquakes could have on fault slip and earthquake activity in the longer-term.

We assessed the impact of the combined co-seismic stress changes on the recurrence interval of each fault by calculating the notional advance or delay time of future earthquakes on each of the faults from the 30 earthquakes modelled from 1349-2016 AD. By analyzing the combined co-seismic stresses for all 30 earthquakes alongside the total accumulated interseismic stresses from 1349-2016 (Figure 8a) we calculated the time advance or delay to the next earthquake, ΔT, at the end of the earthquake sequence using the equation:

$$\Delta T = \frac{\sum_{n=1}^{30} \Delta CFF_n}{CFF_i} \quad (2)$$

where ΔCFF_n is the mean co-seismic stress change on a fault following earthquake *n* and CFF_i is the interseismic loading rate. The advance or delay of future earthquakes due to the co-seismic stress changes for all earthquakes on each fault is plotted in Figure 8b and Figure 9. The summed effect of the co-seismic stress changes for 30 earthquakes can advance or delay the expected timings of earthquakes by thousands of years (Figure 9).

To investigate potential structural controls on the impact of fault interactions on short timescales, we analysed whether fault length or fault orientation affect the advance or delay of future earthquakes (Figures 10 and S4). Figure 10 shows how shorter faults are more prone to advances or delays in future earthquakes times than longer faults. This appears to follow the relationship between fault loading rates and fault length that shows that longer faults have faster interseismic loading rates (Figure 3e). Moreover, the standard deviation of advance or delay times is also greater for shorter faults: recurrence intervals for shorter faults are more variable on both an individual fault basis and across the whole fault system. In contrast, there appears to be no systematic relationship between overall fault orientation and the advance or delay of future earthquakes in our model (Figure S4).

The results shown in Figures 4-10 are for an example scenario where slip-rates averaged since 15 ka for each fault are used to drive the model of interseismic stress accumulation and the M=5.8 earthquake in 1456 AD is on the Maiella Fault and the 1654 AD earthquake is on the Cassino Fault. The results for the alternative model runs including varying the fault slip-rates between 12 ka and 18 ka (the uncertainty on the age of the measured fault offsets), locations of the 1456 and 1654 AD earthquakes and the magnitude of the historical earthquakes are shown in Figure S5. Whilst the results section above and discussion below refer to the results and figures shown in the main body of this paper, the discussions and conclusions hold irrespective of the iteration of the earthquake location, fault slip-rate, or historical earthquake magnitude variations used (Figure 10d and Figure S5).

5 Discussion

We show that earthquake inter-event times on 97 individual faults become highly variable over the course of 30 earthquakes across the region, despite imposing linear interseismic loading. We show, using the exceptional record of historical earthquakes in central Italy, that the combination of interseismic loading over 667 years and the co-seismic Coulomb stress changes from 30 earthquakes produces a statistically significant correspondence between the location of previous earthquakes and subsequent seismic events. We demonstrate the importance of co-seismic stress shadows on perturbing the earthquake recurrence, particularly, of short faults. We argue that our results show how fault length plays a key role in the effects of fault interaction. These findings are discussed in the context of what we can learn from this natural example about how fault systems behave over timescales of 10^2-10^3 years.

Of the 21 earthquakes from 1654, all but one event occurred on faults where the mean combined interseismic and co-seismic stress was positive (Figure 7). This is despite 21-26% of faults being negatively stressed at any one time. This positive result for 20 events confirms the strong association between positive Coulomb stress change and earthquake occurrence observed by other authors [e.g. *Deng and Sykes*, 1997; *Stein et al.*, 1997]. Furthermore, the use of a statistical Mann-Whitney U test enables us to reject the (null) hypothesis that the stresses on the faults that failed fall within a random pattern within the distribution of stresses on all the faults.

Our approach of imposing continuous creep in deep shear zones to set long-term fault slip-rates (Figure 3a-c) leads to some faults having higher interseismic loading rates (Figure 3d). The two longest faults have the highest loading rates because these faults have the highest measured Holocene throws (and thus slip rates) across them and many of the shorter faults are loaded at lower rates (although the correlation is not strong $R^2 = 0.25$; Figure 3e). Whilst this result is due to our model setup (Figure 3), a physical explanation for this difference is that ductile deformation is likely to be more localized down-dip of large faults and less localized down-dip of smaller faults. Such behavior is typical in a material with a non-linear viscous rheology as has been inferred for the central Apennines [*Cowie et al*., 2013].

Given that the co-seismic stress changes are only 1-2 orders of magnitude greater than the interseismic loading rates of ~10^{-2}-10^{-3} MPa yr^{-1}, it would be expected that after c. 10-100 years, negative co-seismic stresses would be eclipsed by interseismic loading stresses. However, throughout the timescale modelled, c. 20% of the faults are consistently experiencing negative stresses (considering both interseismic and co-seismic stress changes; Figure 6 and Figure 7b). This may be due to the apparent cluster of earthquakes in the area surrounding the L'Aquila valley during the last 667 years. Earthquakes occurred in this area in 1461, 1703 (2nd February) and 2009, and the concentration of relatively short faults across strike from the L'Aquila valley results in these faults having their stress decreased following each of the events (Figure 6). Whilst the importance of stress shadows has been noted before [e.g. *Harris and Simpson*, 1998], by resolving stress changes on individual faults, we show the importance of stress shadows on perturbing the recurrence times of short faults with low interseismic loading rates (Figure 9-10). It takes longer for the interseismic loading stresses to overcome the negative co-seismic stresses on shorter faults given their generally lower interseismic stress loading rates (Figure 10 and Figure 3e). In addition, due to the comparative size of the stress shadows, it appears that negative co-seismic Coulomb stresses have a greater impact on *delaying* fault recurrence intervals compared with the advancement of fault recurrence intervals by positive co-seismic Coulomb stresses (Figure 10). Therefore, although the role of stress triggering in earthquake clustering over short time-scales (i.e. days-c.10 years) is well documented [e.g. *Stein et al*. 1994], it does not appear that Coulomb stress changes alone can cause the significant *accelerations* in fault slip-rate over thousands of years revealed by ^{36}Cl data long bedrock fault scarps in the central Apennines [e.g. *Cowie et al*. 2017]. However, Coulomb stress changes are effective at *delaying* future earthquakes by thousands of years, especially on shorter faults (Figure 9-10).

The sensitivity of small faults to slip-rate perturbations has been observed in both theoretical and real fault systems. Palaeoseismic data from normal faults in the Taupo Rift, New Zealand shows that faults with lower slip-rates experience greater variations in displacement rate through time [*Nicol et al.*, 2010] and numerical simulations of fault interactions suggest the percentage of across strike strain accommodated by a fault (which is analogous to fault slip-rate) affects the slip-rate variability [*Cowie et al.*, 2012]. Figure 10 shows how the stress perturbations modelled have a greater effect on both the recurrence times (Figure 10b), and the variance in recurrence times (Figure 10c) of shorter faults. The dependence between slip rate variability and fault length has only been observed in extensional regions, and therefore

may not apply to localized, plate-boundary faults. However, the systematic variations in earthquake recurrence intervals with fault length that arise not only in our model of the last 667 years in central Italy, but also in observations from New Zealand, suggests that in extensional regions, Coulomb stress interactions play an important role in influencing irregular earthquake recurrence intervals over thousands of years. Elastic stress interactions therefore provide a plausible physical explanation for the mechanism controlling observations of greater fault slip rate variability on shorter faults that is not readily explained by other possible causes of slip-rate variability.

The effects of Coulomb stress interactions on smaller faults only becomes apparent due to the detail of the fault map used in our model which includes all (97) major faults in the region. In contrast, other studies often simplify the major faults a region (e.g. *Robinson et al.* [2004; 2009] in the Taupo Rift and *Marzocchi et al.* [2009] and *Marzocchi and Melini*, [2014] in central Italy) or only resolve stress changes on a small number of faults (e.g.; *Li et al.* [2015] in the Shanxi Rift, China, and *Verdecchia and Carena*, [2016] in eastern California and western Nevada). By resolving stress changes on all faults in the region, we were able to explore the characteristics of the complicated interactions in areas of distributed faulting.

Our modelling suggests that the largescale fault orientation appears to have little or no systematic control on the magnitude of fault interaction (Figure S4) over timescales of 10^1-10^3 years (i.e. beyond aftershock sequences). It appears at the current stage of development of the fault system (i.e. beyond incipient localization), fault location has become more important than fault orientation on controlling fault interactions [e.g. *Cowie*, 1998].

As fault location appears to be more important than fault orientation on the impacts of stress interactions, areas with a greater density of shorter faults may be more likely to be susceptible to the impacts of Coulomb stress changes. *Nicol et al*. [2010] suggested that the activity of the shortest faults in the Taupo Rift is controlled by the largest earthquakes in the region (i.e. the earthquakes that occurred on the largest faults). In contrast, in the offshore part of the Taupo Rift, the spatial distribution of short faults is varied, with localized deformation and associated long faults in the southwest of the Whakatane Graben, and distributed deformation and a higher density of short faults in the northeast of the region [*Nixon et al*., 2014]. In this example, the shorter faults that are most susceptible to Coulomb stress changes are not situated in the areas where the largest earthquakes could occur as they are not adjacent to the

longest faults. Therefore, more moderate sized earthquakes may cause greater perturbations in earthquake recurrence intervals as these earthquakes occur in areas surrounded by a higher density of shorter faults. This may explain why earthquakes in the central Apennines since 1349 have clustered on the northeastern side of the mountain range (Figure 1c): there appears to be a higher density of faulting in this region, especially surrounding the L'Aquila valley, yet the historical earthquakes are of a more moderate magnitude (M6-M6.7; Figure 2a). In contrast, the southwest of the region has hosted the largest magnitude earthquakes (e.g. the M_e7.0 1915 earthquake) and may have a higher proportion of longer faults (Figure 2a).

6 Conclusions

The central Apennines, similar to many other areas of extensional tectonics, show evidence of spatially variable earthquake clusters and temporally variable fault slip-rates over 10's to thousands of years. To investigate the role of elastic fault interactions in controlling these observations we modelled the co-seismic and interseismic Coulomb stress changes for 30 earthquakes in central Italy over 667 years on all active faults in the region.

We demonstrate that with a simple model that uses linear inputs for interseismic stress accumulation based on real measurements of the rate of movements of faults, co-seismic Coulomb stress changes caused by the 30 earthquakes lead to highly non-linear outputs. Our model illustrates how Coulomb stress changes can account for variability in the earthquake recurrence intervals of faults of hundreds to thousands of years.

Despite the interseismic loading stresses being on the order of $<10^{-2}$ MPa yr^{-1} and co-seismic stress changes being on the order of 10^{-1} MPa for each event, co-seismic stress shadows are a pervasive feature of the sequence of earthquakes modelled with approximately 20% of faults negative stress shadows at any one time. We also find that the pattern of faults that fail in each earthquake is not random, rather earthquakes are more likely to occur on faults with higher levels of Coulomb stress.

We calculated the earthquake delay or advance due to co-seismic Coulomb stress changes and find that earthquakes can be advanced or delayed by hundreds to thousands of years. Furthermore, the susceptibility of faults to delays or advances in recurrence times appears to vary systematically with fault length (Figure 10). Faults with lower interseismic loading rates, which are generally the shorter faults, are more susceptible to co-seismic Coulomb stress

changes when compared to the longest faults in the array. This behavior has been observed in other extensional tectonic settings around the world suggesting that, Coulomb stress interactions play an important role in controlling variable earthquake recurrence intervals in these settings and the magnitude of this effect may be a function of fault length.

Acknowledgements

This work was funded by a UCL Impact Studentship with CASE support from Geospatial Research Limited and support from the UCL Institute for Risk and Disaster Reduction [LW], NERC Urgency Grant NE/P018858/1 [LW, GR and KM], and NERC standard grants NE/I024127/1 (GR and PS) and NE/I026715/1 (KM). We thank Laura Gregory, John McCloskey and Katerina Stavrianaki for comments and discussions on early versions of this work. Most figures were prepared using the GMT software [*Wessel and Smith*, 1995]. We thank the reviews from Ross Stein and an anonymous reviewer, which significantly improved this manuscript. All data for this paper is properly cited and referred to in the reference list.

References

Akçar, N., D. Tikhomirov, Ç. Özkaymak, S. Ivy-Ochs, V. Alfimov, H. Sözbilir, B. Uzel, and C. Schlüchter (2012), 36Cl exposure dating of paleoearthquakes in the Eastern Mediterranean: First results from the western Anatolian Extensional Province, Manisa fault zone, Turkey, *Geol. Soc. Am. Bull.*, *124*(11-12), 1724–1735, doi:10.1130/B30614.1.

Aki, K. (1984), Asperities, Barriers, Characteristic Earthquakes and Strong Motion Prediction, *J. Geophys. Res.*, *89*(B7), 5867, doi:10.1029/JB089iB07p05867.

Aki, K., and P. G. Richards (1980), *Quantitative Seismology*, 2nd Editio., University Science Books.

Begg, J. G., and V Mouslopoulou (2010), Analysis of late Holocene faulting within an active rift using lidar, Taupo Rift, New Zealand, *Journal of Volcanology and Geothermal Research*, *190*(1-2), 152-167, doi: 10.1016/j.jvolgeores.2009.06.001.

Benedetti, L., R. Finkel, D. Papanastassiou, G. King, R. Armijo, F. Ryerson, D. Farber, and F. Flerit (2002), Post-glacial slip history of the Sparta fault (Greece) determined by 36Cl cosmogenic dating: Evidence for non-periodic earthquakes, *Geophys. Res. Lett.*, *29*(8), doi: 10.1029/2001GL014510, doi:10.1029/2001GL014510.

Benedetti, L., I. Manighetti, Y. Gaudemer, R. Finkel, J. Malavieille, K. Pou, M. Arnold, G. Aumaître, D. Bourlès, and K. Keddadouche (2013), Earthquake synchrony and clustering on Fucino faults (Central Italy) as revealed from in situ 36Cl exposure dating, *J. Geophys. Res. Solid Earth*, *118*(9), 4948–4974, doi:10.1002/jgrb.50299.

Blumetti, A. (1995), Neotectonic investigations and evidence of paleoseismicity in the epicentral area of the January–February 1703, Central Italy, earthquakes, *Perspect. Paleoseismology, Assoc. Eng. Geol. Bull. Spec. Publ.*, *6*, 83–100.

Boncio, P., G. Lavecchia, and B. Pace (2004), Defining a model of 3D seismogenic sources for Seismic Hazard Assessment applications: the case of central Apennines (Italy), *J. Seismol.*, *8*, 407–425, doi:10.1023/B:JOSE.0000038449.78801.05.

Boncio, P., D. P. Tinari, G. Lavecchia, F. Visini, and G. Milana (2009), The instrumental seismicity of the Abruzzo Region in Central Italy (1981-2003): Seismotectonic Implications, *Ital. J. Geosci. (Bollettino della Soc. Geol. Ital. e del Serv. Geol. d'Italia)*, *128*(2), 367–380, doi:10.3301/IJG.2009.128.2.367.

Brodsky, E. E., and N. J. van der Elst (2014), The Uses of Dynamic Earthquake Triggering, *Annu. Rev. Earth Planet. Sci.*, *42*, 317-339, doi: 10.1146/annurev-earth-060313-054648.

Bull, J. M., P. M. Barnes, G. Lamarche, D. J. Sanderson, P. A. Cowie, S. K. Taylor, and J. K. Dix (2006), High-resolution record of displacement accumulation on an active normal fault: implications for models of slip accumulation during repeated earthquakes, *J. Struct. Geol.*, *28*(7), 1146–1166, doi:10.1016/j.jsg.2006.03.006.

Cello, G., S. Mazzoli, E. Tondi, and E. Turco (1997), Active tectonics in the central Apennines and possible implications for seismic hazard analysis in peninsular Italy, *Tectonophysics*, *272*(1), 43–68.

Cello, G., G. Deiana, P. Mangano, S. Mazzoli, E. Tondi, L. Ferreli, L. Maschio, A. M. Michetti, L. Serva, and E. Vittori (1998), Evidence for surface faulting during the September 26, 1997, Colfiorito (central Italy) earthquakes, *J. Earthq. Eng.*, *2*(2), 303–324, doi:10.1080/13632469809350324.

Chiarabba, C. et al. (2009), The 2009 L'Aquila (central Italy) M W 6.3 earthquake: Main shock and aftershocks, *Geophys. Res. Lett.*, *36*(18), L18308, doi:10.1029/2009GL039627.

Cinti, F. R., D. Pantosti, G. D'Addezio, and P. M. De Martini (1992), Paleosismicità della faglia Ovindoli-Pezza (Abruzzo), in *Atti 11° Convegno Annuale GNGTS, Roma, 9-11 Dicembre 1992*, pp. 273–285.

Cinti, F. R., D. Pantosti, P. M. De Martini, S. Pucci, R. Civico, S. Pierdominici, L. Cucci, C. a. Brunori, S. Pinzi, and A. Patera (2011), Evidence for surface faulting events along the Paganica fault prior to the 6 April 2009 L'Aquila earthquake (central Italy), *J. Geophys. Res.*, *116*(B7), B07308, doi:10.1029/2010JB007988.

Cowie, P. A. (1998), A healing–reloading feedback control on the growth rate of seismogenic faults, *J. Struct. Geol.*, *20*(8), 1075–1087, doi:10.1016/S0191-8141(98)00034-0.

Cowie, P. A., and G. P. Roberts (2001), Constraining slip rates and spacings for active normal faults, *J. Struct. Geol.*, *23*(12), 1901–1915, doi:10.1016/S0191-8141(01)00036-0.

Cowie, P. A., C. Vanneste, and D. Sornette (1993), Statistical physics model for the spatiotemporal evolution of faults, *J. Geophys. Res.*, *98*(B12), 21809, doi:10.1029/93JB02223.

Cowie, P. A., J. R. Underhill, M. D. Behn, J. Lin, and C. E. Gill (2005), Spatio-temporal evolution of strain accumulation derived from multi-scale observations of Late Jurassic rifting in the northern North Sea: A critical test of models for lithospheric extension, *Earth Planet. Sci. Lett.*, *234*(3-4), 401–419, doi:10.1016/j.epsl.2005.01.039.

Cowie, P. A., G. P. Roberts, J. M. Bull, and F. Visini (2012), Relationships between fault

geometry, slip rate variability and earthquake recurrence in extensional settings, *Geophys. J. Int.*, *189*(1), 143–160, doi:10.1111/j.1365-246X.2012.05378.x.

Cowie, P. A., C. H. Scholz, G. P. Roberts, J. P. Faure Walker, and P. Steer (2013), Viscous roots of active seismogenic faults revealed by geologic slip rate variations, *Nat. Geosci.*, *6*(12), 1036–1040, doi:10.1038/ngeo1991.

Cowie, P. A. el al. (2017), Orogen-scale uplift in the central Italian Apennines drives episodic behaviour of earthquake faults, *Sci. Rep.*, *7*, 44858, doi:10.1038/srep44858.

D'Addezio, G., E. Masana, and D. Pantosti (2001), The Holocene paleoseismicity of the Aremogna-Cinque Miglia Fault (Central Italy), *J. Seismol.*, *5*, 181–205, doi:10.1023/A:1011403408568.

D'Agostino, N. (2014), Complete seismic release of tectonic strain and earthquake recurrence in the Apennines (Italy), *Geophys. Res. Lett.*, *41*(4), 1155–1162, doi:10.1002/2014GL059230.

D'Agostino, N., J. A. Jackson, F. Dramis, and R. Funiciello (2001), Interactions between mantle upwelling, drainage evolution and active normal faulting: an example from the central Apennines (Italy), *Geophys. J. Int.*, *147*(2), 475–497, doi:10.1046/j.1365-246X.2001.00539.x.

D'Agostino, N., S. Mantenuto, E. D'Anastasio, R. Giuliani, M. Mattone, S. Calcaterra, P. Gambino, and L. Bonci (2011), Evidence for localized active extension in the central Apennines (Italy) from global positioning system observations, *Geology*, *39*(4), 291–294, doi:10.1130/G31796.1.

Das, S., and C. H. Scholz (1983), Why large earthquakes do not nucleate at shallow depth, *Nature*, *305*(September), 621–623, doi:10.1038/305621a0.

Deng, J., and L. R. Sykes (1997), Evolution of the stress field in southern California and triggering of moderate-size earthquakes: A 200-year perspective, *J. Geophys. Res.*, *102*(B5), 9859, doi:10.1029/96JB03897.

Dolan, J. R., D. D. Bowman, and C. G. Sammis (2007), Long-rage and long-term fault interactions in Southern California, *Geology*, *35*(9), 855, doi: 10.1130/G23789A.1.

Dolan, J. F., L. J. McAuliffe, E. J. Rhodes, S. F. McGill, and R. Zinke (2016), Extreme multi-millennial slip rate variations on the Garlock fault, California: Strain super-cycles, potentially time-variable fault strength, and implications for system-level earthquake occurrence, *Earth Planet. Sci. Lett.*, *446*, 123-136, doi: 10.1016/j.epsl.2016.04.011.

Faure Walker, J. P., G. P. Roberts, P. A. Cowie, I. D. Papanikolaou, P. R. Sammonds, A. M. Michetti, and R. J. Phillips (2009), Horizontal strain-rates and throw-rates across breached relay zones, central Italy: Implications for the preservation of throw deficits at points of normal fault linkage, *J. Struct. Geol.*, *31*(10), 1145–1160, doi:10.1016/j.jsg.2009.06.011.

Faure Walker, J. P., G. P. Roberts, P. R. Sammonds, and P. Cowie (2010), Comparison of earthquake strains over 10^2 and 10^4 year timescales: Insights into variability in the seismic cycle in the central Apennines, Italy, *J. Geophys. Res.*, *115*(B10), B10418, doi:10.1029/2009JB006462.

Faure Walker, J. P., G. P. Roberts, P. A. Cowie, I. Papanikolaou, A. M. Michetti, P. Sammonds, M. Wilkinson, K. J. W. McCaffrey, and R. J. Phillips (2012), Relationship

between topography, rates of extension and mantle dynamics in the actively-extending Italian Apennines, *Earth Planet. Sci. Lett.*, *325-326*, 76–84, doi:10.1016/j.epsl.2012.01.028.

Field, E. H., D. D. Jackson, and J. F. Dolan (1999), A mutually consistent seismic-hazard source model for Southern California, *Bull. Seismol. Soc. Am.*, *89*(3), 559–578.

Friedrich, A. M., B. P. Wernicke, N. A. Niemi, R. A. Bennett, and J. L. Davis (2003), Comparison of geodetic and geologic data from the Wasatch region, Utah, and implications for the spectral character of Earth deformation at periods of 10 to 10 million years, *J. Geophys. Res.*, 108(B4), 1-23, doi: 10.1029/2001JB000682

Galadini, F., and P. Galli (1999), The Holocene paleoearthquakes on the 1915 Avezzano earthquake faults (central Italy): implications for active tectonics in the central Apennines, *Tectonophysics*, *308*(1-2), 143–170, doi:10.1016/S0040-1951(99)00091-8.

Galadini, F., and P. Galli (2003), Paleoseismology of silent faults in the Central Apennines (Italy): the Mt. Vettore and Laga Mts. faults, *Ann. Geophys.*, *46*(5), 815–836, doi:10.4401/ag-3457.

Galadini, F., P. Galli, and C. Giraudi (1997), Geological investigations of Italian earthquakes: New paleoseismological data from the fucino plain (Central Italy), *J. Geodyn.*, *24*(1-4), 87–103, doi:10.1016/S0264-3707(96)00034-8.

Galadini, F., P. Messina, B. Giaccio, and A. Sposato (2003a), Early uplift history of the Abruzzi Apennines (central Italy): Available geomorphological constraints, *Quat. Int.*, *101-102*, 125–135, doi:10.1016/S1040-6182(02)00095-2.

Galadini, F., P. Galli, and M. Moro (2003b), Paleoseismology of silent faults in the Central Apennines (Italy): the Campo Imperatore Fault (Gran Sasso Range Fault System), *Ann. Geophys.*, *46*(October), 793–813, doi:10.4401/ag-3456.

Galli, P., and R. Comassi (2009), Rapporto sugli effetti del terremoto aquilano del 6 aprile, *Rapporto congiunto DPC-INGV*, 12pp: http://www.protezionecivile.gov.it/resources/cms/documents/Elenco_centri_abiati_danneggiati.pdf (accessed May 2015).

Galli, P., and F. Galadini (2003), Disruptive earthquakes revealed by faulted archaeological relics in Samnium (Molise, southern Italy), *Geophys. Res. Lett.*, *30*(5), 1266, doi:10.1029/2002GL016456.

Galli, P. A. C., and J. A. Naso (2009), Unmasking the 1349 earthquake source (southern Italy): paleoseismological and archaeoseismological indications from the Aquae Iuliae fault, *J. Struct. Geol.*, *31*(2), 128–149, doi:10.1016/j.jsg.2008.09.007.

Galli, P., F. Galadini, M. Moro, and C. Giraudi (2002), New paleoseismological data from the Gran Sasso d'Italia area (central Apennines), *Geophys. Res. Lett.*, *29*(7), 1134, doi:10.1029/2001GL013292.

Galli, P., F. Galadini, and F. Calzoni (2005), Surface faulting in Norcia (central Italy): a "paleoseismological perspective," *Tectonophysics*, *403*(1-4), 117–130, doi:10.1016/j.tecto.2005.04.003.

Galli, P., B. Giaccio, and P. Messina (2010), The 2009 central Italy earthquake seen through 0.5 Myr-long tectonic history of the L'Aquila faults system, *Quat. Sci. Rev.*, *29*(27-28), 3768–3789, doi:10.1016/j.quascirev.2010.08.018.

Galli, P. A. C., B. Giaccio, P. Messina, E. Peronace, and G. M. Zuppi (2011), Palaeoseismology of the L'Aquila faults (central Italy, 2009, Mw 6.3 earthquake): implications for active fault linkage, *Geophys. J. Int.*, *187*(3), 1119–1134, doi:10.1111/j.1365-246X.2011.05233.x.

Galli, P., B. Giaccio, E. Peronace, and P. Messina (2015), Holocene Paleoearthquakes and Early-Late Pleistocene Slip Rate on the Sulmona Fault (Central Apeninnes, Italy), *Bull. Seismol. Soc. Am.*, *105*(1), 1–13, doi:10.1785/0120140029.

Galli, P., E. Pronace, F. Bramerini, S. Castenetto, G. Naso, F. Cassone, F. Pallone (2016), The MCS intensity distribution of the devastating 24 August 2016 earthquakes in central Italy (Mw 6.2), *Ann. Di Geofis.*, 59 (Fast Track 5), doi:10.4401/ag-7287.

Gasperini, P., and G. Ferrari (2000), Deriving numerical estimates from descriptive information: the computation of earthquake parameters, *Ann. Di Geofis.*, *43*(4), 729–746, doi:10.4401/ag-3670.

Giraudi, C., and M. Frezzotti (1995), Palaeoseismicity in the Gran Sasso Massif (Abruzzo, Central Italy), *Quat. Int.*, *25*(94), 81–93, doi:10.1016/1040-6182(94)P3716-L.

Gold, R. D., E. Cowgill, J. R. Arrowsmith, A. M. Friedrich (2017), Pulsed strain release on the Altyn Tagh fault, northwest China, *Earth Planet. Sci. Lett.*, *459*, 291-300, doi: 10.1016/j.epsl.2016.11.024.

Guidoboni, E., G. Ferrari, D. Mariotti, A. Comastri, G. Tarabusi, and G. Valensise (2007), CFTI4Med, Catalogue of Strong Earthquakes in Italy (461 B.C.-1997) and Mediterranean Area (760 B.C.-1500), *INGV-SGA.* Available from: http://storing.ingv.it/cfti4med/ (Accessed 26 May 2015)

Guidoboni, E., A. Comastri, D. Mariotti, C. Ciuccarelli, and M. G. Bianchi (2012), Ancient and Medieval Earthquakes in the Area of L'Aquila (Northwestern Abruzzo, Central Italy), A.D. 1-1500: A Critical Revision of the Historical and Archaeological Data, *Bull. Seismol. Soc. Am.*, *102*(4), 1600–1617, doi:10.1785/0120110173.

Harris, R. A., and R. W. Simpson (1998), Suppression of large earthquakes by stress shadows: A comparison of Coulomb and rate-and-state failure, *J. Geophys. Res.*, *103*(B10), 24439, doi:10.1029/98JB00793.

Hetzel, R., and A. Hampel (2005), Slip rate variations on normal faults during glacial-interglacial changes in surface loads. *Nature*, *435*, 81-84, doi: 10.1038/nature03562.

Huc, M., R. Hassani, and J. Chéry (1998), Large earthquake nucleation associated with stress exchange between middle and upper crust, *Geophys. Res. Lett.*, *25*(4), 551–554, doi:10.1029/98GL00091.

Jewell, P. W., and R. L. Bruhn (2013), Evaluation of Wasatch fault segmentation and slip rates using Lake Bonneville shorelines, *J. Geophys. Res.*, *118*(5), 2528-2543, doi: 10.1002/jgrb.50174.

King, G. C. P., R. S. Stein, and J. Lin (1994), Static stress changes and the triggering of earthquakes, *Bull. Seismol. Soc. Am.*, *84*(3), 935–953.

Kostrov, V. V. (1974), Seismic moment and energy of earthquakes and seismic flow of rocks, *Izv. Earth Phys.*, *1*, 23–40.

Li, B., M. B. Sørensen, and K. Atakan (2015), Coulomb stress evolution in the Shanxi rift system, North China, since 1303 associated with coseismic, post-seismic and

interseismic deformation, *Geophys. J. Int.*, *203*(3), 1642–1664, doi:10.1093/gji/ggv384.

Lin, J., and R. S. Stein (2004), Stress triggering in thrust and subduction earthquakes and stress interaction between the southern San Andreas and nearby thrust and strike-slip faults, *J. Geophys. Res.*, *109*(B2), B02303, doi:10.1029/2003JB002607.

Livio, F., A. M. Michetti, E. Vittori, L. Gregory, L. Wedmore, L. Piccardi, and Central Italy Working Group (2016), Surface faulting during the August 24, 2016, Central Italy earthquake (Mw 6.0): preliminary results, *Ann. Di Geofis.*, 59 (Fast Track 5), doi:10.4401/ag-7197.

Maniatis, G., and A. Hampel (2008), Along-strike variations of the slip direction on normal faults: Insights from three-dimensional finite-element models, *J. Struct. Geol.*, *30*(1), 21–28, doi:10.1016/j.jsg.2007.10.002.

Manighetti, I., M. Campillo, C. Sammis, P. M. Mai, and G. King (2005), Evidence for self-similar, triangular slip distributions on earthquakes: Implications for earthquake and fault mechanics, *J. Geophys. Res.*, *110*(B5), B05302, doi:10.1029/2004JB003174.

Manighetti, I., M. Campillo, S. Bouley, and F. Cotton (2007), Earthquake scaling, fault segmentation, and structural maturity, *Earth Planet. Sci. Lett.*, *253*(3–4), 429–438, doi:10.1016/j.epsl.2006.11.004.

Marzocchi, W., and D. Melini (2014), On the earthquake predictability of fault interaction models, *Geophys. Res. Lett.*, *41*(23), 8294–8300, doi:10.1002/2014GL061718.

Marzocchi, W., J. Selva, F. R. Cinti, P. Montone, S. Pierdominici, R. Schivardi, and E. Boschi (2009), On the occurrence of large earthquakes: New insights from a model based on interacting faults embedded in a realistic tectonic setting, *J. Geophys. Res.*, *114*(B1), B01307, doi:10.1029/2008JB005822.

Michetti, A. M., F. Brunamonte, L. Serva, and E. Vittori (1996), Trench investigations of the 1915 Fucino earthquake fault scarps (Abruzzo, central Italy): Geological evidence of large historical events, *J. Geophys. Res.*, *101*(B3), 5921, doi:10.1029/95JB02852.

Michetti, A. M., L. Ferreli, E. Esposito, S. Porfido, A. M. Blumetti, E. Vittori, L. Serva, and G. P. Roberts (2000), Ground Effects during the 9 September 1998 Mw = 5.6, Lauria Earthquake and the Seismic Potential of the "Aseismic" Pollino Region in Southern Italy, *Seismol. Res. Lett.*, *71*(1), 31–46, doi:10.1785/gssrl.71.1.31.

Mitchell, S. G., A. Matmon, P. R. Bierman, Y. Enzel, M. Caffee, and D. Rizzo (2001), Displacement history of a limestone normal fault scarp, northern Israel, from cosmogenic ^{36}Cl, *J. Geophys. Res.*, *106*(B3), 4247, doi:10.1029/2000JB900373.

Morewood, N. C., and G. P. Roberts (2000), The geometry, kinematics and rates of deformation within an en echelon normal fault segment boundary, central Italy, *J. Struct. Geol.*, *22*(8), 1027–1047, doi:10.1016/S0191-8141(00)00030-4.

Moro, M., V. Bosi, F. Galadini, P. Galli, B. Giaccio, P. Messina, and A. Sposato (2002), Analisi Paleosismologiche Lungo La Faglia del M. Marine (alta Valle Dell'Aterno): Risultati Preliminari, *Quat.*, *15*(2), 259–270.

Nalbant, S., J. McCloskey, S. Steacy, M. NicBhloscaidh, and S. Murphy (2013), Interseismic coupling, stress evolution, and earthquake slip on the Sunda megathrust, *Geophys. Res. Lett.*, *40*(16), 4204–4208, doi:10.1002/grl.50776.

Nalbant, S. S., A. Hubert, and G. C. P. King (1998), Stress coupling between earthquakes in

northwest Turkey and the north Aegean Sea, *J. Geophys. Res.*, *103*(B10), 24469, doi:10.1029/98JB01491.

Nicol, A., J. J. Walsh, P. Villamor, H. Seebeck, and K. R. Berryman (2010), Normal fault interactions, paleoearthquakes and growth in an active rift, *J. Struct. Geol.*, *32*(8), 1101–1113, doi:10.1016/j.jsg.2010.06.018.

Nicol, A., R Robinson, R. Van Dissen, and A Harvison (2016), Variability of recurrence interval and single-event slip for surface rupturing earthquakes in New Zealand, *New Zealand Journal of Geology and Geophysics*, *59*(1), 97-116, doi 10.1080/00288306.2015.1127822.

Nixon, C. W., J. M. Bull, and D. J. Sanderson (2014), Localized vs distributed deformation associated with the linkage history of an active normal fault, Whakatane Graben, New Zealand, *J. Struct. Geol.*, *69*, 266–280, doi:10.1016/j.jsg.2014.06.005.

Noda, H., N Lapusta, and H. Kanamori (2013), Comparison of average stress drop measures for ruptures with heterogeneous stress change and implications for earthquake physics, *Geophys. J. Int.*, *193*(3), 1691-1712, doi:10.1093/gji/ggt074.

Okada, Y. (1992), Internal Deformation Due to Shear and Tensile Faults in a Half-Space, *Bull. Seismol. Soc. Am.*, *82*(2), 1018–1040.

Olson, E. L., and R. M. Allen (2005), The deterministic nature of earthquake rupture, *Nature*, *438*(7065), 212–215, doi:10.1038/nature04214.

Olson, E. L., and R. M. Allen (2006), Earth science: Is earthquake rupture deterministic? (Reply), *Nature*, *442*(7100), E6–E6, doi:10.1038/nature04964.

Oskin, M., L Perg, E Shelef, M Strane, E. Gurney, B. Singer, and X Zhang (2008), Elevated shear zone loading rate during an earthquake cluster in eastern California, *Geology*, *36*(6), 507-510, doi: 10.1130/G24814A.1.

Pace, B., P. Boncio, and G. Lavecchia (2002), The 1984 Abruzzo earthquake (Italy): an example of seismogenic process controlled by interaction between differently oriented synkinematic faults, *Tectonophysics*, *350*(3), 237–254, doi:10.1016/S0040-1951(02)00118-X.

Pace, B., L. Peruzza, G. Lavecchia, and P. Boncio (2006), Layered Seismogenic Source Model and Probabilistic Seismic-Hazard Analyses in Central Italy, *Bull. Seismol. Soc. Am.*, *96*(1), 107–132, doi:10.1785/0120040231.

Palumbo, L., L. Benedetti, D. Bourlès, A. Cinque, and R. Finkel (2004), Slip history of the Magnola fault (Apennines, Central Italy) from 36Cl surface exposure dating: evidence for strong earthquakes over the Holocene, *Earth Planet. Sci. Lett.*, *225*(1-2), 163–176, doi:10.1016/j.epsl.2004.06.012.

Pantosti, D., G. D'Addezio, and F. R. Cinti (1996), Paleoseismicity of the Ovindoli-Pezza fault, central Apennines, Italy: A history including a large, previously unrecorded earthquake in the Middle Ages (860–1300 A.D.), *J. Geophys. Res.*, *101*(B3), 5937, doi:10.1029/95JB03213.

Papanikolaou, I. D., G. P. Roberts, and A. M. Michetti (2005), Fault scarps and deformation rates in Lazio–Abruzzo, Central Italy: Comparison between geological fault slip-rate and GPS data, *Tectonophysics*, *408*(1-4), 147–176, doi:10.1016/j.tecto.2005.05.043.

Roberts, G. P., and A. M. Michetti (2004), Spatial and temporal variations in growth rates

along active normal fault systems: an example from The Lazio–Abruzzo Apennines, central Italy, *J. Struct. Geol.*, *26*(2), 339–376, doi:10.1016/S0191-8141(03)00103-2.

Roberts, G. P., A. M. Michetti, P. A. Cowie, N. C. Morewood, and I. Papanikolaou (2002), Fault slip-rate variations during crustal-scale strain localisation, central Italy, *Geophys. Res. Lett.*, *29*(8), 1168, doi:10.1029/2001GL013529.

Roberts, G. P., P. Cowie, I. Papanikolaou, and A. M. Michetti (2004), Fault scaling relationships, deformation rates and seismic hazards: an example from the Lazio–Abruzzo Apennines, central Italy, *J. Struct. Geol.*, *26*(2), 377–398, doi:10.1016/S0191-8141(03)00104-4.

Robinson, R. (2004), Potential earthquake triggering in a complex fault network: The northern South Island, New Zealand, *Geophys. J. Int.*, *159*(2), 734–748, doi:10.1111/j.1365-246X.2004.02446.x.

Robinson, R., A. Nicol, J. J. Walsh, and P. Villamor (2009), Features of earthquake occurrence in a complex normal fault network: Results from a synthetic seismicity model of the Taupo Rift, New Zealand, *J. Geophys. Res.*, *114*(12), B12306, doi:10.1029/2008JB006231.

Rydelek, P., and S. Horiuchi (2006), Earth science: Is earthquake rupture deterministic?, *Nature*, *442*(7100), E5–E6, doi:10.1038/nature04963.

Salvi, S., F. R. Cinti, L. Colini, G. D'Addezio, F. Doumaz, and E. Pettinelli (2003), Investigation of the active Celano-L'Aquila fault system, Abruzzi (central Apennines, Italy) with combined ground-penetrating radar and palaeoseismic trenching, *Geophys. J. Int.*, *155*(3), 805–818, doi:10.1111/j.1365-246X.2003.02078.x.

Schlagenhauf, A., I. Manighetti, L. Benedetti, Y. Gaudemer, R. Finkel, J. Malavieille, and K. Pou (2011), Earthquake supercycles in Central Italy, inferred from 36Cl exposure dating, *Earth Planet. Sci. Lett.*, *307*(3–4), 487–500, doi:10.1016/j.epsl.2011.05.022.

Scholz, C. H. (1994), Reply to comments on 'A reappraisal of large earthquake scaling', *Bull. Seismol. Soc. Am.*, 84, 1677.

Scholz, C. H. (2002), *The Mechanics of Earthquakes and Faulting*, Cambridge University Press.

Steacy, S., D. Marsan, S. S. Nalbant, and J. McCloskey (2004), Sensitivity of static stress calculations to the earthquake slip distribution, *J. Geophys. Res.*, *109*(B4), B04303, doi:10.1029/2002JB002365.

Stein, R. S., G. C. P. King, and J. Lin (1992), Change in Failure Stress on the Southern San Andreas Fault System Caused by the 1992 Magnitude = 7.4 Landers Earthquake, *Science (80-.).*, *258*(5086), 1328–1332, doi:10.1126/science.258.5086.1328.

Stein, R. S., G. C. P. King, and J. Lin (1994), Stress Triggering of the 1994 M=6.7 Northridge, California, Earthquake by its Predecessors, *Science*, *265*(5177), 1432-1435, doi:10.1126/science.265.5177.1432

Stein, R. S., A. A. Barka, and J. H. Dieterich (1997), Progressive failure on the North Anatolian fault since 1939 by earthquake stress triggering, *Geophys. J. Int.*, *128*(3), 594–604, doi:10.1111/j.1365-246X.1997.tb05321.x.

Tertulliani, A., L. Cucci, A. Rossi, and V. Castelli (2012), The 6 October 1762 Middle Aterno Valley (L'Aquila, Central Italy) Earthquake: New Constraints and New Insights,

Seismol. Res. Lett., *83*(6), 1068–1077, doi:10.1785/0220120048.

Tesson, J., B., Pace, L. Benedetti, F. Visini, M. Delli Rocioli, M. Arnold, G. Aumaître, D. L. Bourlès, and K. Keddadouche (2016), Seismic slip history of the Pizzalto fault (Central Apennines, Italy) using in situ-produced ^{36}Cl cosmic ray exposure dating and rare earth element concentrations., *J. Geophys. Res. Solid Earth*, n/a-n/a, doi:10.1002/2015JB012565.

Toda, S., R. S. Stein, K. Richards-Dinger, and S. B. Bozkurt (2005), Forecasting the evolution of seismicity in southern California: Animations built on earthquake stress transfer, *J. Geophys. Res. Solid Earth*, *110*(5), 1–17, doi:10.1029/2004JB003415.

Tucker, G. E., S. W. McCoy, A. C. Whittaker, G. P. Roberts, S. T. Lancaster, and R. Phillips (2011), Geomorphic significance of postglacial bedrock scarps on normal-fault footwalls, *J. Geophys. Res. Earth Surf.*, *116*(F1), F01022, doi:10.1029/2010JF001861.

Verdecchia, A. and S. Carena (2016), Coulomb stress evolution in a diffuse plate boundary: 1400 years of earthqakes in eastern California and western Nevada, USA, *Tectonics*, 35, doi:10.1002/2015TC004091.

Walters, R. J., J. R. Elliott, N. D'Agostino, P. C. England, I. Hunstad, J. A. Jackson, B. Parsons, R. J. Phillips, and G. Roberts (2009), The 2009 L'Aquila earthquake (central Italy): A source mechanism and implications for seismic hazard, *Geophys. Res. Lett.*, *36*(17), L17312, doi:10.1029/2009GL039337.

Weldon, R, K. Scharer, T. Fumal, and G. Biasi (2004), Wrightwood and the earthquake cycle: What a long recurrence record tells us about how faults work, *Geological Society of America Today*, *14*(9), 4-10, doi:10.1130/1052-5173(2004)014<4:WATECW>2.0CO;2.

Wells, D. L., and K. J. Coppersmith (1994), New Empirical Relationships among Magnitude, Rupture Length, Rupture Width, Rupture Area, and Surface Displacement, *Bull. Seismol. Soc. Am.*, *84*(4), 974–1002.

Wessel, P., and W. J. F. Smith (1995), New version of the generic mapping tools released, *EOS Trans. Am. Geophys. Union*, *76*(33), 329, doi:10.1029/95EO00198.

Westaway, R., R. Gawthorpe, and M. Tozzi (1989), Seismological and field observations of the 1984 Lazio-Abruzzo earthquakes: implications for the active tectonics of Italy, *Geophys. J. Int.*, *98*(3), 489–514, doi:10.1111/j.1365-246X.1989.tb02285.x.

Whittaker, A. C., P. A. Cowie, M. Attal, G. E. Tucker, and G. P. Roberts (2007), Bedrock channel adjustment to tectonic forcing: Implications for predicting river incision rates, *Geology*, *35*(2), 103, doi:10.1130/G23106A.1.

Wilkinson, M. et al. (2015), Slip distributions on active normal faults measured from LiDAR and field mapping of geomorphic offsets: an example from L'Aquila, Italy, and implications for modelling seismic moment release, *Geomorphology*, *237*, 130–141, doi:10.1016/j.geomorph.2014.04.026.

Zöller, G., and S. Hainzl (2007), Recurrence Time Distributions of Large Earthquakes in a Stochastic Model for Coupled Fault Systems: The Role of Fault Interaction, *Bull. Seismol. Soc. Am.*, *97*(5), 1679–1687, doi:10.1785/0120060262.

Table 1: Historical earthquakes. The details of each of the historical earthquake included within this study. The date and magnitude of each event are taken from the Italian CFTI catalogue [*Guidoboni et al*. 2007]. The inferred causative fault of each of the events and the literature sources for this inference are also listed.

Date	Magnitude[b]	Inferred Fault Rupture	Source
9th September 1349	6.8	Pozzilli Fault	*Galli and Naso* [2009]
9th September 1349	6.0	Aremogna Cinque-Miglia Fault	*D'Addezio et al.* [2001]
9th September 1349	6.1	Fiamignano Fault	Historical records[a]; *Guidoboni et al.* [2012]
5th December 1456[c]	7.0	Bojano and Carpino Isernia Faults	*Galli and Galadini* [2003]
5th December 1456	5.8	Sulmona Fault? Mailella Fault?	*Guidoboni et al.* [2012]
27th November 1461	6.4	Paganica Fault	*Galli et al.* [2011]
6th November 1599	6.0	Atri and Cascia Faults	Historical records[a]
8th October 1639	6.1	Laga Mt Gorzano Fault	*Boncio et al.* [2004]
15th October 1639	6.2	Laga Mt Gorzano Fault	*Boncio et al.* [2004]
24th July 1654	6.3	Liri Fault? Cassino Fault?	Historical Records[a]
14th January 1703	6.7	Norcia, Norcia Antithetic and Mt Alvegnano Faults	*Blumetti* [1995]
16th January 1703	6.0	Montereale Fault	*Blumetti* [1995]
2nd February 1703	6.7	Barete and Paganica Faults	*Galli et al.* [2010], *Cinti et al.* [2011]
3rd November 1706	6.8	Maeilla and Palena Faults	Historical Records[a]
12th May 1730	5.9	Norcia Fault	Historical Records[a]; *Blumetti* [1995]
6th October 1762	5.3	San Demetrio Fault	*Tertulliani et al.* [2012]
26th July 1805[c]	6.6	Bojano Fault	Historical Records[a]; *Galli and Galadini* [2003]
22nd August 1859	5.8	Norcia Fault	Historical records[a]
24th February 1904	5.6	Magliano dei Marsi Fault	Historical records[a]
13th January 1915	7.0	Fucino, Parasano and San Sebastiano Faults	*Michetti et al.* [1996]
26th September 1933	6.0	Maiella Fault	Historical records[a]; *Marzocchi et al.* [2009]
19th September 1979	5.8	Mt Alvegnano Fault	*Blumetti* [1995]
7th May 1984	5.8	Barrea Fault	*Westaway et al.* [1989]; *Pace et al.* [2002]

26th September 1997[c]	5.7	Colfiorito Fault	*Cello et al.* [1998]
26th September 1997 [c]	6.0	Colfiorito and Costa Corgnetto Faults	*Cello et al.* [1998]
14th October 1997 [c]	5.6	Costa Corgnetto Fault	*Cello et al.* [1998]
6th April 2009	6.3	Paganica Fault	*Walters et al.* [2009]
24th August 2016	6.2	Laga and Mt Vettore Fault	*Livio et al.* [2016]
26th October 2016	6.1	Mt Vettore Fault (Mt Bove seg.)	Observed in field
30th October 2016	6.6	Mt Vettore Fault	Observed in field

[a]Refers to the macroseismic shaking records listed in *Guidoboni et al.* [2007].

[b]The magnitudes of earthquakes that occurred prior to 1979 AD are listed in the Catalogue di Forti Terremoti [*Guidoboni et al.*, 2007] and are derived from the macroseismic shaking records using the *Boxer* code of *Gasperini and Ferrari* [2000] and as such are described as equivalent magnitudes (M_e). For more recent earthquakes (1979-2016 AD) the magnitudes described are from seismological sources.

[c]These earthquakes occurred at the extreme north-west and south-east of the study region. They were included to ensure faults are not affected by edge effects in the modelling of fault interactions, however, they are not included within the analysis in Figure 1c and later Figures (Figures 8-10 and Figure S4).

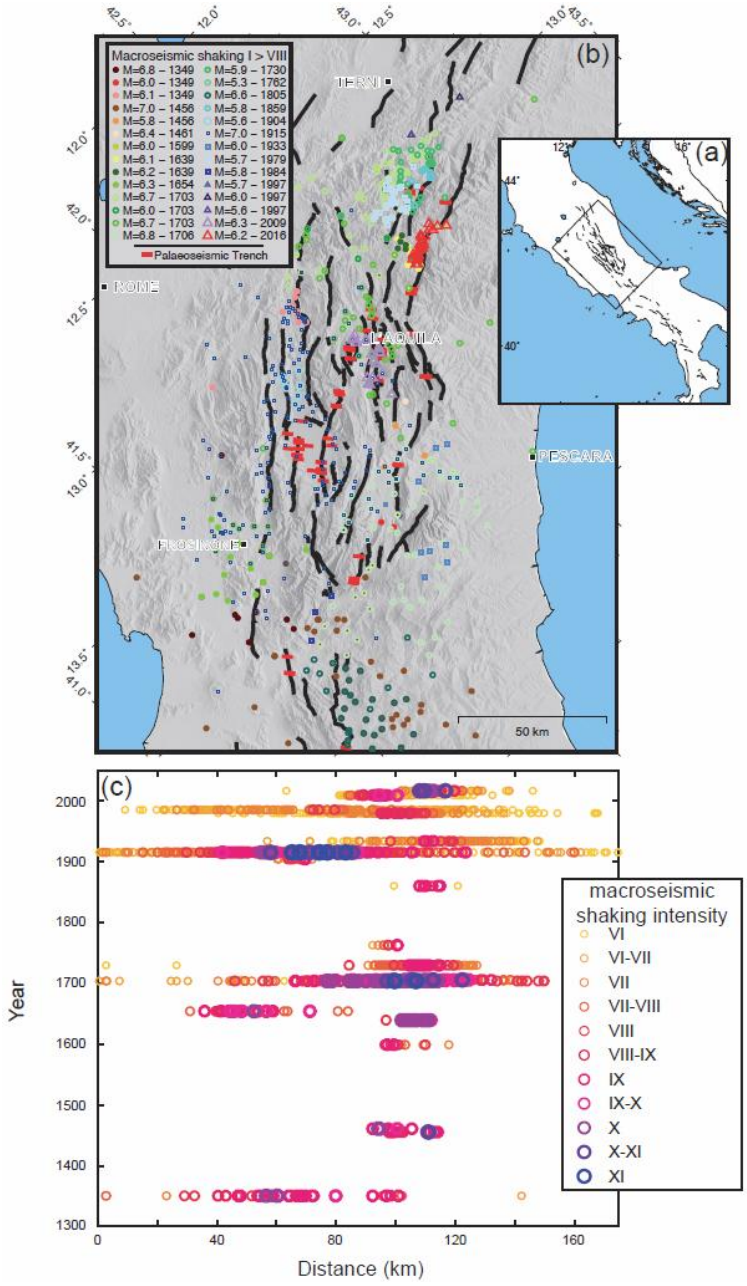

Figure 1. Historical earthquake shaking in the central Apennines. (a) The location of the central Apennines fault system within Italy, and the location of the parts b and c. (b) A rotated map of central Italy showing the location of all towns and villages shaken at $I_{mcs} \geq$ VIII by the major historical earthquakes in the region from 1349 to the Mw=6.2 earthquake in 2016. The active faults in the region are shown with black lines, and the palaeoseismic trenches dug across these faults are shown with red lines. (c) The macroseismic shaking ($I_{mcs} \geq$ VI) for each historical earthquake projected onto a transect orientated perpendicular to the mean strike of faults in the central Apennines (225°). Macroseismic data from *Guidoboni et al*. [2007], *Galli and Comasssi* [2009] and *Galli et al*. [2016]. Macroseismic data for the two earthquakes in October 2016 were not available at the time of submission.

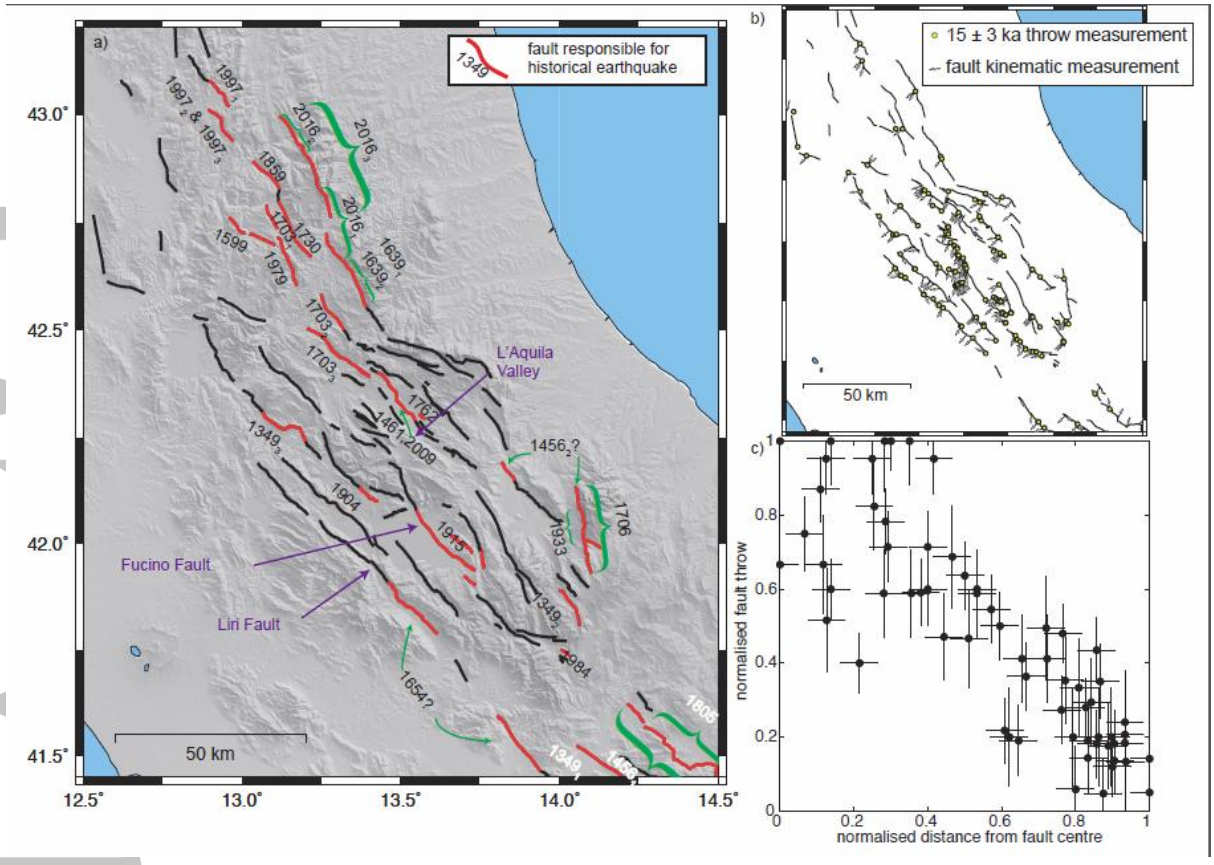

Figure 2. Earthquakes and fault kinematics in the central Apennines. (a) The inferred locations of fault ruptures for all earthquakes from 1349-2016. The earthquakes and magnitudes are listed in Table 1. (b) The location where offset of 15 ± 3 ka geomorphic features gives the throw rate of the faults in the central Apennines, and the locations where the kinematics of the faults have been measured (and the kinematic direction). (c) A comparison of finite fault throw profiles from faults in the central Apennines using data from [*Roberts and Michetti*, 2004]. Each measurement has been normalised to both the distance from the centre of each fault and the maximum throw measurement of each fault.

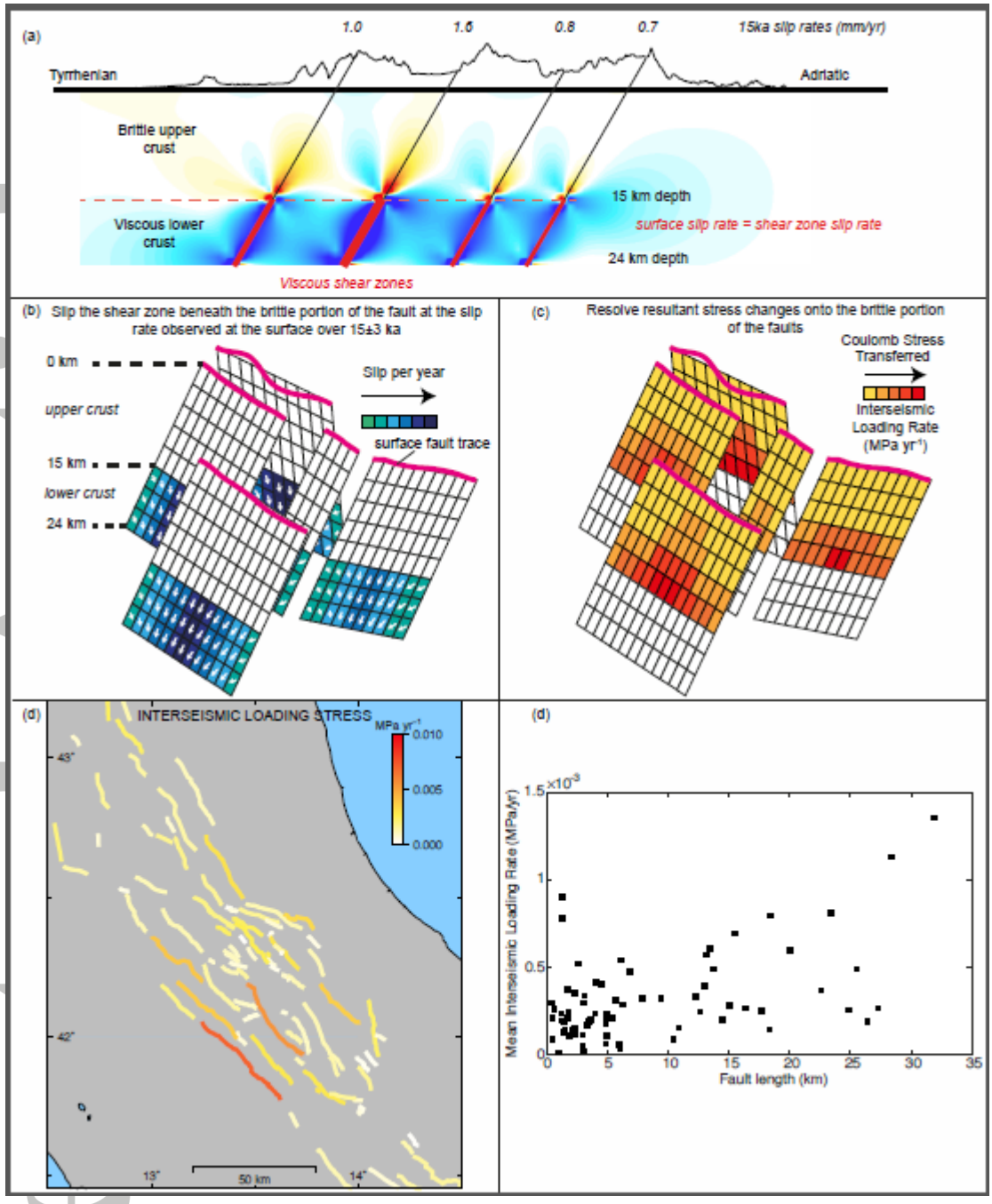

Figure 3. Modelling interseismic stress accumulation. (a) Faults are loaded by slip in viscous shear zones beneath the seismogenic crust. (b) The slip rate in the shear zone beneath each fault is based on the measured surface strain-rate over 15 ± 3 ka. (c) The stress changes caused by slip in the shear zones are resolved onto patches of fault above 15km depth, in the brittle portion of the crust. (d) The maximum interseismic loading stress modelled shown projected onto the surface trace of each fault. (e) The change in mean interseismic loading rate with fault length.

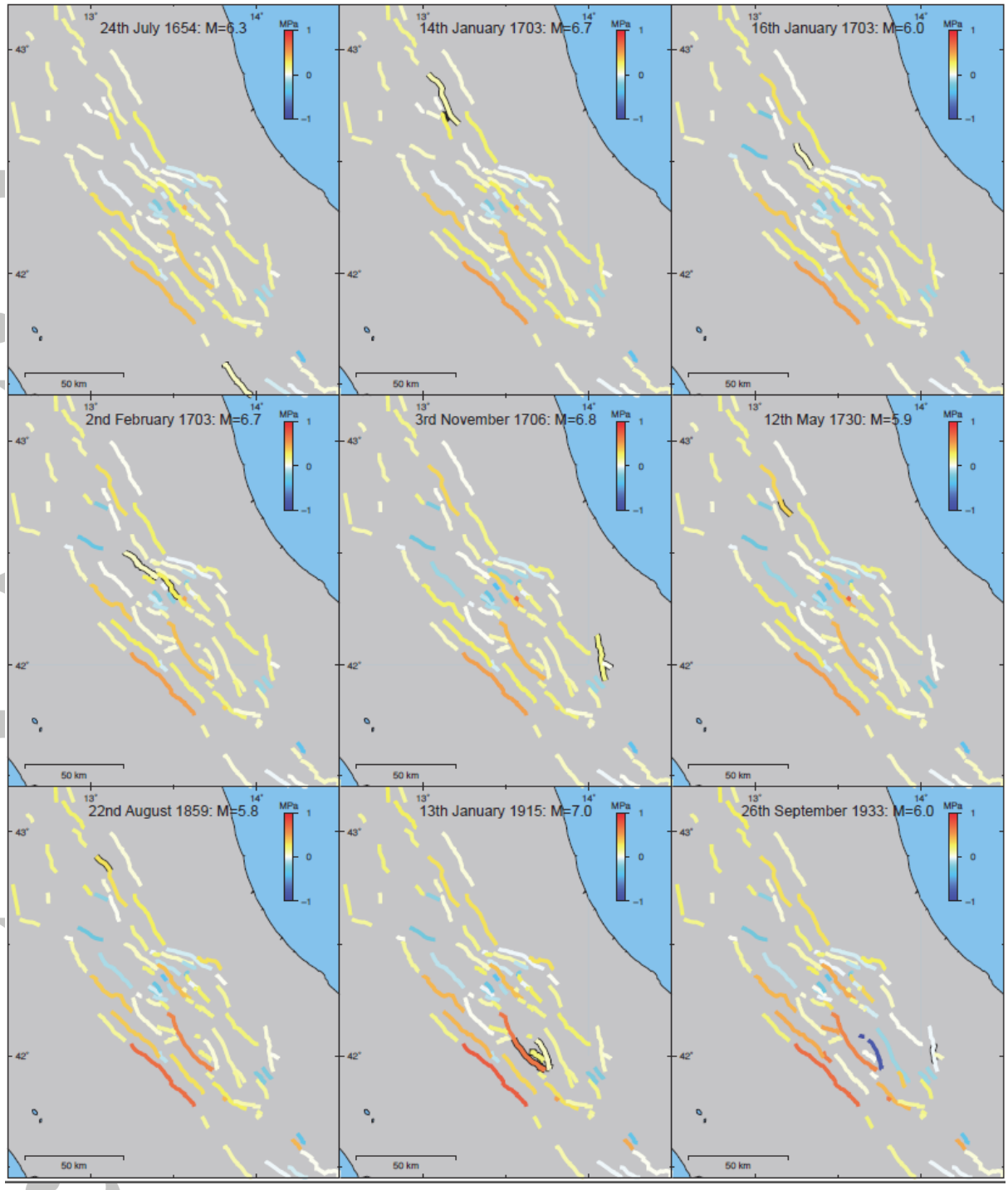

Figure 4. The mean Coulomb stress on faults prior to each earthquake from 1654-1933. Earthquakes that are included in the modelling but occur outside the central Apennines (e.g. the 1805 earthquake) are not shown. The images shown include interseismic and co-seismic Coulomb stress changes that have accumulated from 1349 until immediately prior to each event. The mean stress is plotted on the surface trace of each fault rather than the planar faults used in the model. The fault (or faults) that rupture in each subsequent earthquake is highlighted in black.

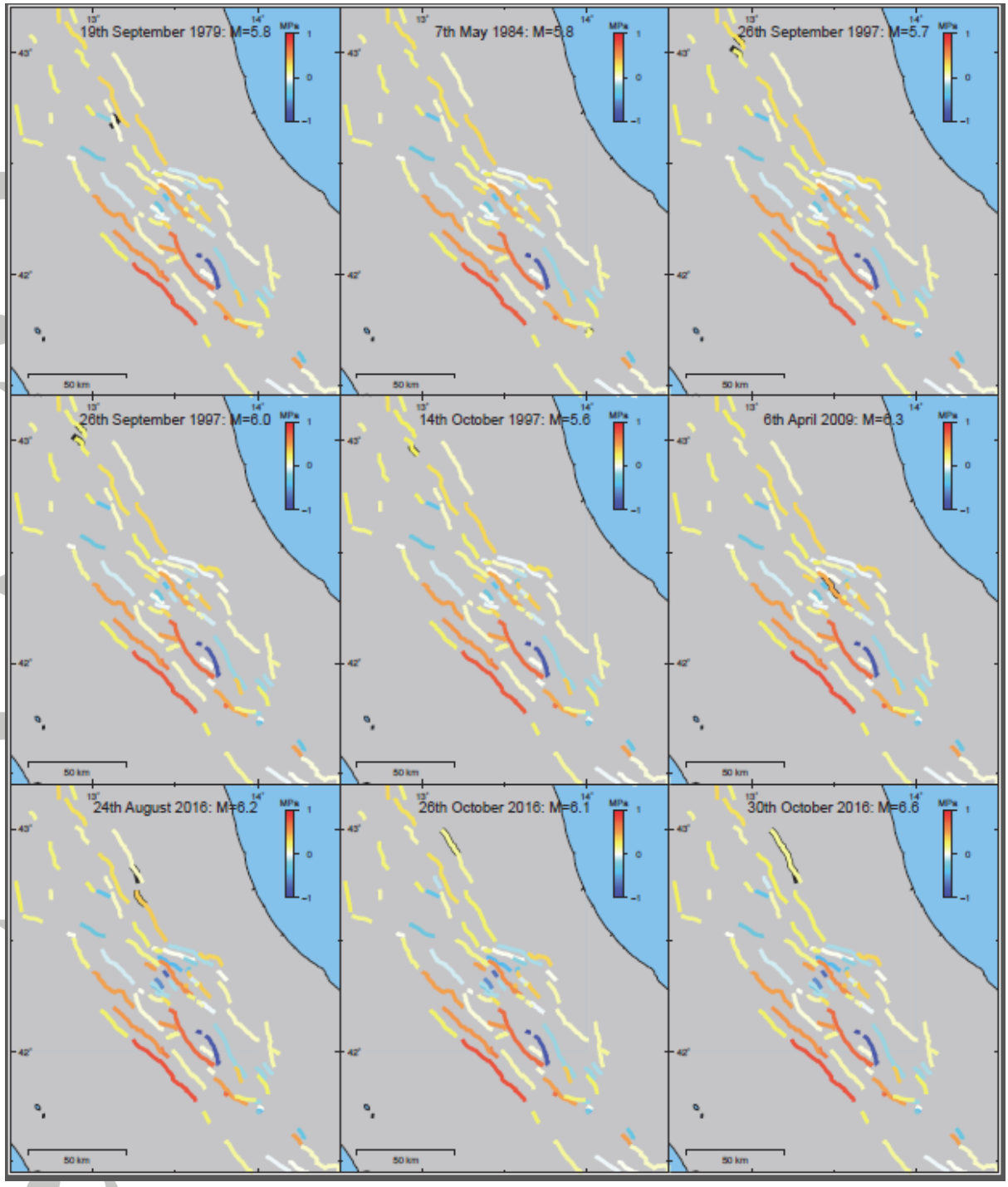

Figure 5. As figure 4 but earthquakes are shown from 1979-2016.

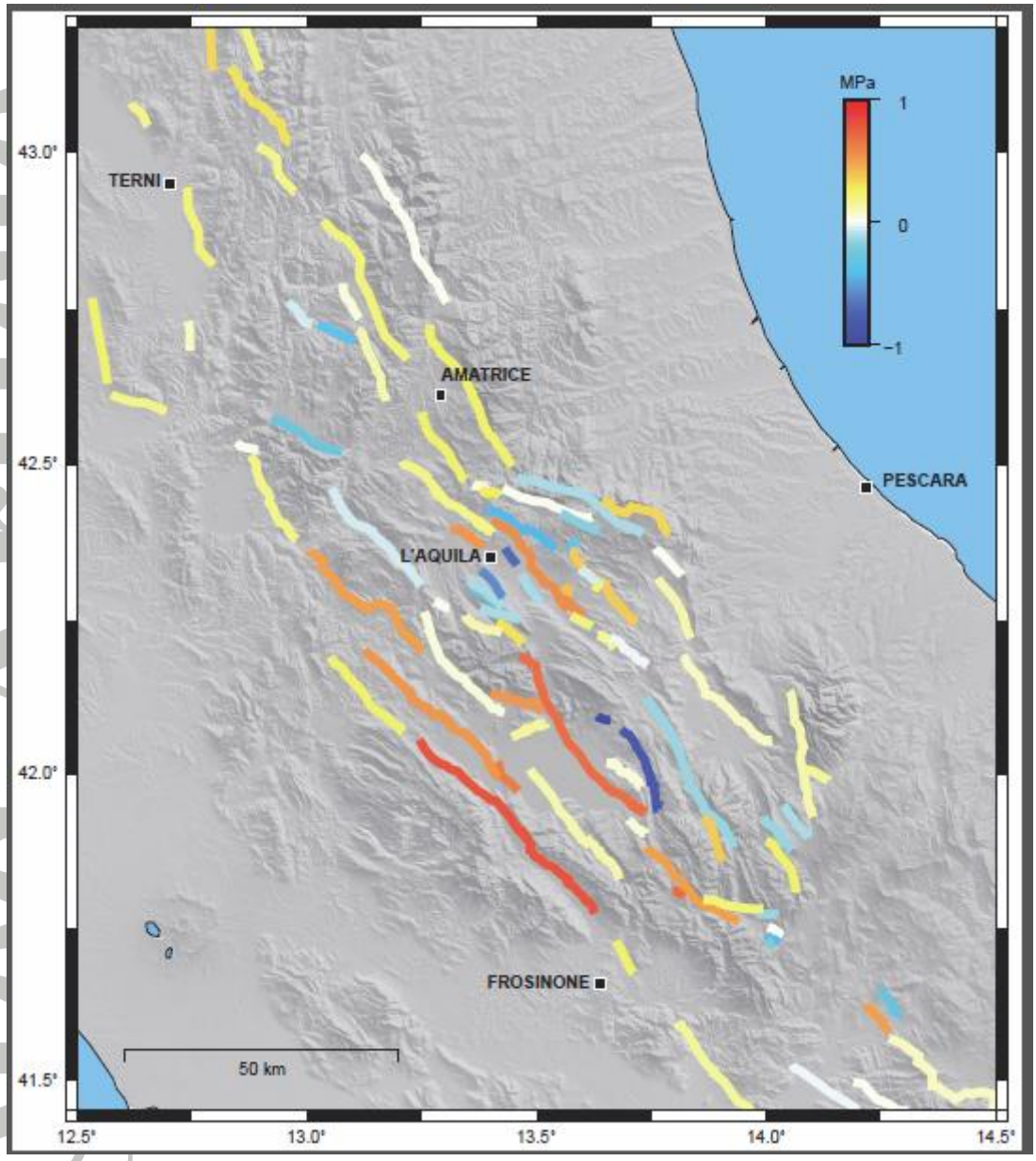

Figure 6. Interseismic and co-seismic Coulomb stress changes from 1349 until after the Mw=6.6 earthquake on 30th October 2016.

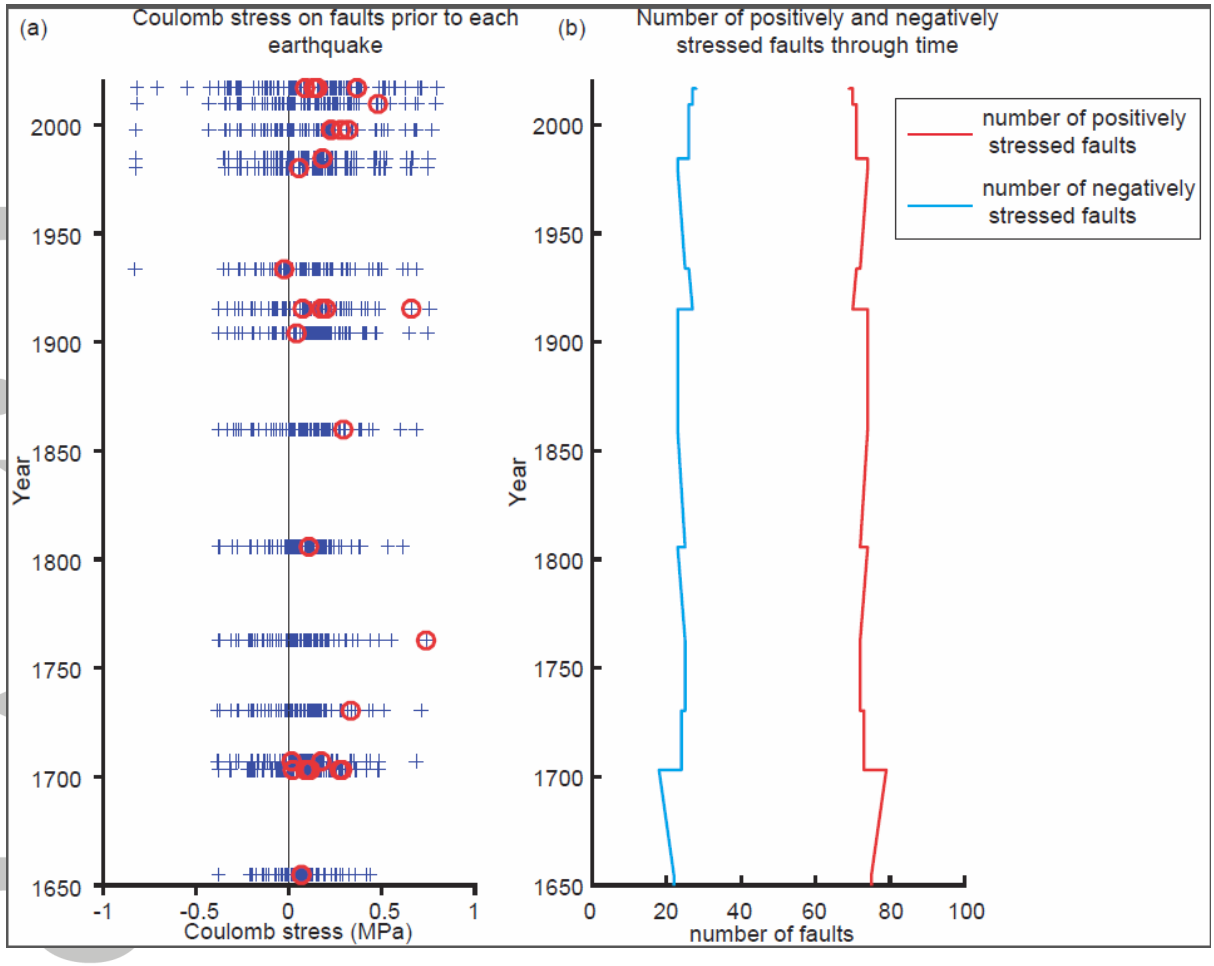

Figure 7. Changes in mean stress on faults through time. (a) The mean Coulomb stress on each fault prior to each earthquake. The blue crosses represent the mean stress on each individual fault. The red circles highlight the faults that subsequently rupture in each event. (b) The number of faults where the mean Coulomb stress (i.e. combined interseismic loading and co-seismic stress changes) is positive and negative through time.

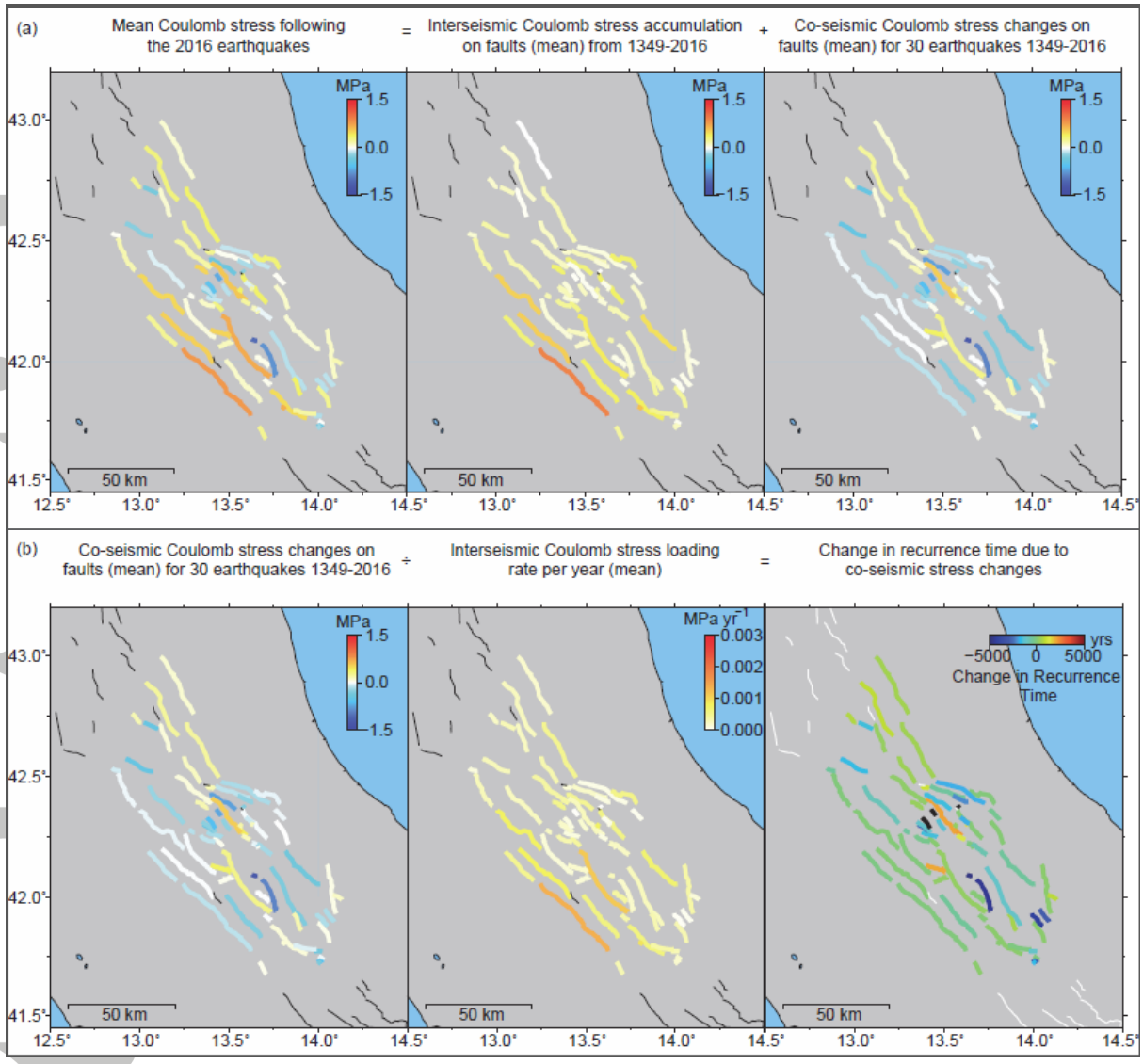

Figure 8. The contributions to the state of stress on all faults following the 2016 Mw=6.6 earthquake and the effects on fault recurrence times (a) The contribution of interseismic and co-seismic stress changes to the stress on each fault following the 2016 Mw=6.6 earthquake. (b) The change in recurrence time of each fault due to the combined co-seismic stress changes from all earthquakes from 1349-2016.

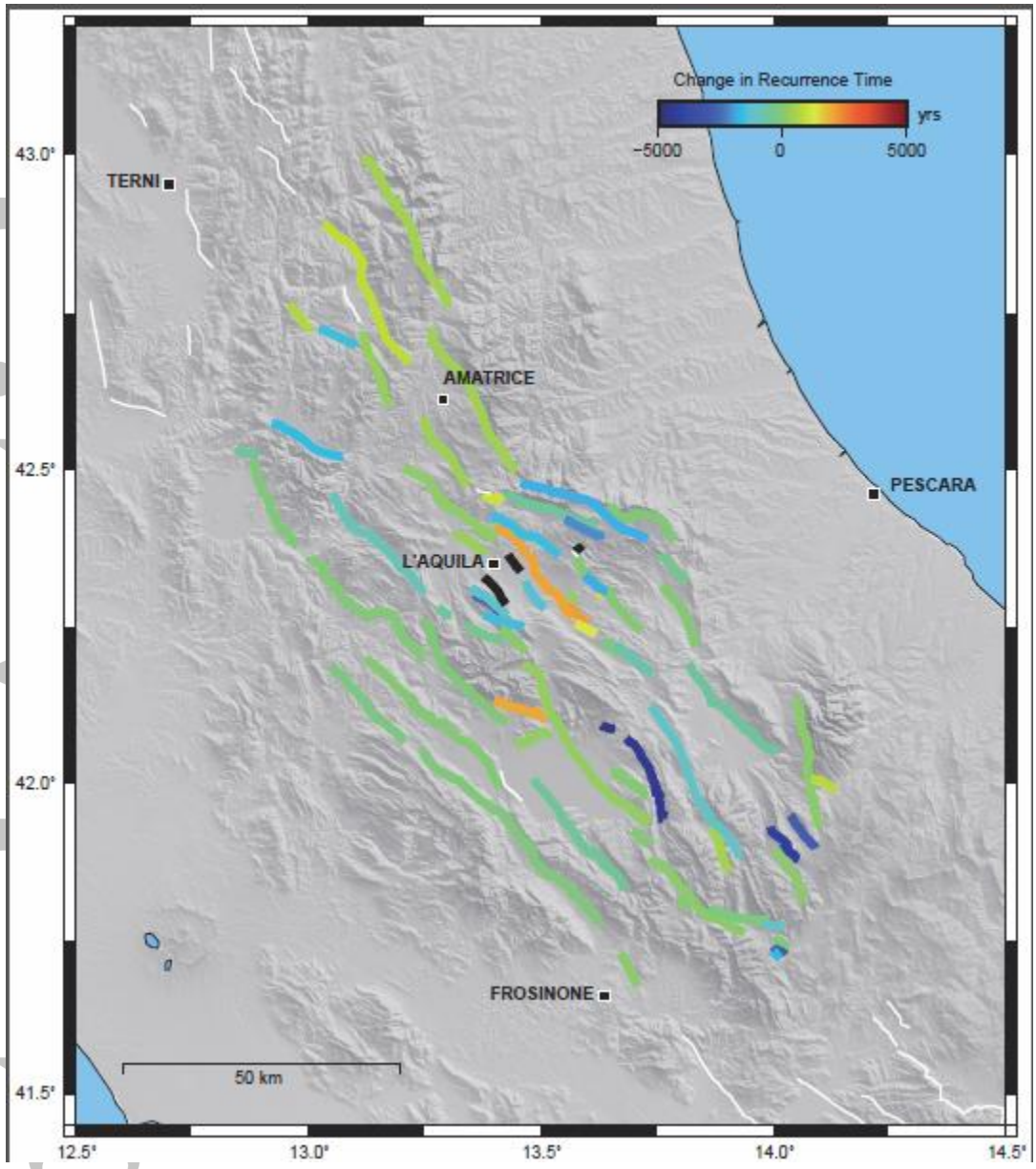

Figure 9. The change in recurrence time of each fault due to the co-seismic Coulomb stress changes of 30 earthquakes from 1349-2016.

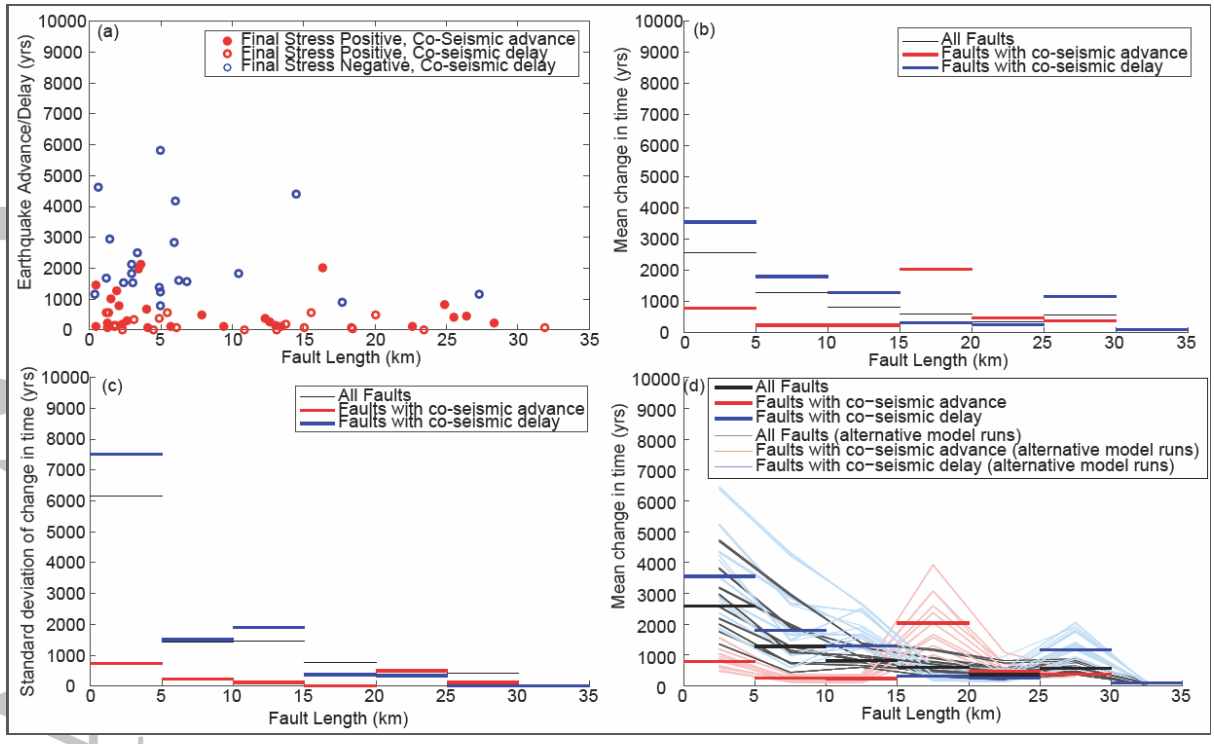

Figure 10. The impact of fault length on earthquake recurrence times (earthquake advance or delay) on individual faults following the 2016 earthquakes. (a) The effect of fault length on the advance or delay of future earthquakes on each fault. The closed red circles show the time the next earthquake on each fault has been advanced by due to co-seismic stress changes where the combined interseismic and co-seismic stresses on the fault is positive following the 2016 earthquakes. The open red circles show the time the delay time of the next earthquake on faults where the combined interseismic and co-seismic stress is positive following the 2016 earthquakes. The open blue circles show the delay time of the next earthquake on faults where the combined stress following the 2016 earthquakes is negative. (b) The mean advance and delay time plotted for faults in 5km bins. (c) The standard deviation in advance and delay times for faults in 5km bins. (d) The same as part a but with alternative model runs shown in the background.